WILEY

Biotechnology and Bioengineering

Isotopomer analysis of myocardial substrate metabolism: A systems biology approach

Journal:	*Biotechnology and Bioengineering*
Manuscript ID:	05-700.R2
Wiley - Manuscript type:	Full Paper
Date Submitted by the Author:	n/a
Complete List of Authors:	Vo, Thuy; University of California, San Diego, Bioengineering Department Palsson, Bernhard; University of California, San Diego, Bioengineering Department
Key Words:	mitochondrial metabolism, non-linear programming, constraint-based modeling, carbon tracer experiments, mass isotopomer analysis, systems biology

Isotopomer analysis of myocardial substrate metabolism: A systems biology approach

Thuy D. Vo[1] and Bernhard O. Palsson[1]

[1]Department of Bioengineering, University of California, San Diego, CA 92093

Running Title: Myocardial flux analysis using ^{13}C labeling data

Key words: cardiac metabolism, mass isotopomer analysis, carbon tracer experiments, constraint-based modeling, nonlinear programming, systems biology

Abbreviations:
AMMs: atom mapping matrices; CAC: citric acid cycle; IMMs: isotopomer mapping matrices; MDVs: mass distribution vectors; ac^{cit}: acetyl-CoA moiety of citrate; oaa^{cit}: oxaloacetate moiety of citrate

Corresponding Author:
Bernhard O. Palsson
Department of Bioengineering
9500 Gilman Dr. 0412
La Jolla, CA 92092-0412
E-mail: bpalsson@be-research.ucsd.edu
Phone: (858) 534-5668
Fax: (858) 822-3120

SUMMARY

The increasing accessibility of mass isotopomer data via GC-MS and NMR technology has necessitated the use of a systematic and reliable method to take advantage of such data for flux analysis. Here we applied a nonlinear, optimization-based method to study substrate metabolism in cardiomyocytes using ^{13}C data from perfused mouse hearts. The myocardial metabolic network used in this study accounts for 257 reactions and 240 metabolites, which are further compartmentalized into extracellular space, cytosol, and mitochondrial matrix. Analysis of the perfused mouse heart showed that the steady state ATP production rate was 16.6 ± 2.3 μmol/min·gww, with 30% of the ATP coming from glycolysis. Of the four substrates available in the perfusate (glucose, pyruvate, lactate, and oleate), exogenous glucose forms the majority of cytosolic pyruvate. Pyruvate decaboxylation is significantly higher than carboxylation, suggesting that anaplerosis is low in the perfused heart. Exchange fluxes were predicted to be high for reversible enzymes in the citric acid cycle, but low in the glycolytic pathway. Pseudoketogenesis amounted to approximately 50% of the net ketone body uptake. Sensitivity analysis showed that the estimated flux distributions were relatively insensitive to experimental errors. The application of isotopomer data drastically improved the estimation of reaction fluxes compared to results computed with respect to reaction stoichiometry alone. Further study of 12 commonly used ^{13}C glucose mixtures showed that the mixtures of 20% [U-$^{13}C_6$] glucose, 80% [3 ^{13}C] glucose and 20% [U-$^{13}C_6$] glucose, 80% [4 ^{13}C] were best for resolving fluxes in the current network.

INTRODUCTION

The quantification of reaction fluxes in cellular metabolism has always been of great interest in physiological and biotechnological research (Nielsen 2003; Yarmush and Berthiaume 1997). Metabolic flux profiles can uncover details about substrate utilization, substrate redistribution at network branch points, and quantitative information about enzyme activity. As intracellular flux measurements tend to be invasive and difficult, our current ability to profile metabolic flux relies on computational tools to analyze experimental data. Studies have shown that isotopomer data, especially ^{13}C tracer data, are useful and effective for estimating intracellular reaction fluxes (Schmidt et al. 1998; Wiechert et al. 1997; Wittmann and Heinzle 1999). In particular, mass isotopomer analysis has been extensively applied to study substrate oxidation and anaplerosis in the heart (Cohen and Bergman 1997; Comte et al. 1997b; Malloy et al. 1996; Panchal et al. 2000), gluconeogenesis (Haymond and Sunehag 2000; Katz and Tayek 1999; Sherry et al. 2004) and lipogenesis in the liver (Bederman et al. 2004; Puchowicz et al. 1999), and activities of the citric acid cycle (CAC) in various tissues (Comte et al. 1997a; Fernandez and Des Rosiers

1995; Katz et al. 1989). Reaction flux estimates in these studies were analytically derived based on observed isotopomer data, assuming a configuration and direction of flux flow in relevant pathways. Such analytical solutions are restricted to small model networks and are not obtainable for many biochemical pathway structures (Klapa et al. 1999). As more isotopomer data become available at a cellular scale, a more general and systemic approach for flux analysis is desirable.

More rigorous modeling methods have been proposed, most of which employ an optimization framework to search for globally optimal flux distributions that produce the observed ^{13}C labeling patterns. Concepts of atom mapping matrices (AMMs) (Zupke and Stephanopoulos 1994), isotopomer mapping matrices (IMMs) (Schmidt et al. 1997), bondomer mapping matrices (van Winden et al. 2002), isotopomer matrices (Forbes et al. 2001), and T matrices (Wiechert et al. 1999) have also been introduced to facilitate the book keeping of different isotopomer states and formulation of balance equations that are amenable to different types of tracer data. Within these formalism, models of various sizes have been developed to study metabolism of *Escherichia coli* (Fischer and Sauer 2003; Schmidt et al. 1999), *Bacillus subtilis* (Dauner et al. 2001), *Methylobacterium extorquens* (Van Dien et al. 2003), *Saccharomyces cerevisiae* (Christensen et al. 2002; Gombert et al. 2001), *Penicillium chrysogenum* (27 reactions (Christensen and Nielsen 2000; van Winden et al. 2003), and *Corynebacterium glutamicum* (Klapa et al. 2003; Marx et al. 1996). In this study, we incorporated isotopomer mapping matrices and isotopomer balance equations into the constraint-based framework to analyze isotopomer data obtained from perfused mouse hearts (Khairallah et al. 2004). Advantages gained from this approach as compared to the use of analytical expressions originally employed by Khairallah et al. (2004) are two fold. First, the use of a cohesive model ensures that estimations of intracellular fluxes are consistent with both isotopomer data and flux measurements obtained from the experiments. The incorporation of known myocardioal metabolic activities and the stoichiometry of underlying biochemical reactions also provides a more complete picture of how the entire cardiomyocyte metabolic network operates and how fluxes in the different pathways fit together. The resulting estimated flux distribution offers a systemic view of the cellular metabolism as supposed to glimpses of fluxes or flux ratios calculated separately and possibly under independent assumptions. Second, the models can be used simulate and analyze experimental scenarios beyond the original experimental conditions. In particular, we used the model to study the effectiveness of 12 different ^{13}C glucose substrate mixtures and identified the most informative metabolites and fluxes to be measured in subsequent experiments. Model contents, computational programs, as well as descriptions of the model building process are available for download at http://systemsbiology.ucsd.edu/organisms.

MATERIALS AND METHODS

Metabolic network and isotopomer analysis

A metabolic network is comprised of reactions and metabolites that are relevant to the metabolic systems or functions of interest. A stoichiometric matrix **S** (240 x 257) (Reed et al. 2006) was constructed to describe the connectivity among 240 metabolites and 257 reactions for the present myocardial metabolic network (Step 1, Table 3). Similar to the previously reconstructed network (Vo et al. 2004), these metabolites and reactions were localized into three compartments: mitochondrial, cytosolic, and extracellular. Atom mapping matrices (Zupke and Stephanopoulos 1994) and isotopomer mapping matrices were employed to track the carbon transfer between products and reactants (Step 2, Table 1). A value of "1" were used instead of fractions for all non-zero A_{ij}, as the convention of using fractions (even for symmetric compounds) as described by Zupke and Stephanopoulos (1994) is inconsistent with the algorithm for computing IMMs from AMMs as developed by Schmidt et al. (1997). The mass balance constraint (Step 3, Table 1) ensured that the time derivative of each metabolite (and isotopomers of each metabolite) in the network equals zero at steady state. The isotopomer balance constraints were algorithmically generated from the stoichiometric matrix and supplied IMMs (Schmidt et al. 1997). Both the forward and the reverse directions of a reversible reaction, which affect the observed isotopomer distributions of the reaction's reactants and products, were incorporated into the isotopomer balance equations. We also transformed these variables as previously described (Arauzo-Bravo and Shimizu 2001; Wiechert and deGraaf 1997). The described constraints and variables were concisely formulated into a nonlinear programming problem, whose objective is to minimize the difference between the measured and the calculated mass distribution (Step 4, Table 1). Values for measured mass isotopomer distributions were corrected for naturally occurring isotopes (Fernandez et al. 1996; Khairallah et al. 2004). We used the sequential quadratic programming (SQP) method (Gill et al. 2002) implemented in the commercially available solver SNOPT (Stanford Business Software, Inc.) to solved the formulated nonlinear programming problem. Contents and computational programs employed in this study are available at http://systemsbiology.ucsd.edu/organisms/.

Sensitivity analysis

The SNOPT solver searches for a locally optimal solution starting from a specified initial point (v_o) in the steady state flux space. In searching for a globally optimal solution, one must sample the entire solution space for locally optimal solutions. The larger the number of locally optimal solutions found, the more likely that one of them is the globally optimal solution. The estimated flux values resulting from these solutions are likely to be sensitive to two parameters: i) the user-defined initial points and ii) the

measured mass distributions ($MDV^{measured}$). The effects of each of these parameters were investigated in our study. The initial values for v_o were generated using two methods. The first method assigned v_o to a flux distribution found by applying a linear programming solver (cplex) with the objective of maximizing or minimizing flux through a chosen reaction in the network. The isotopomer balance constraints (non-linear) were excluded in this step. The second method assigned v_o to a random flux distribution within the convex space, using the Hit-and-Run algorithm (Kaufmann 1998; Thiele et al. 2005). These two methods produced 489 and 1000 unique v_o, respectively.

To investigate the effect of uncertainty associated with each isotopomer measurement, we generated 100 random hypothetical measurements (for each mass isotopomer of each metabolite) drawn from normal distributions having the reported mean and standard error. Randomly selected values from these measurement pools produced 100 *hypothetical* mass distribution data sets based on measurement statistics (see supplemental data for details). We repeated the flux calculation to evaluate how these mass distributions affected the predicted flux distributions.

RESULTS

I) ANALYSIS OF THE MOUSE CARDIOMYOCYTE

We have reconstructed a metabolic network for the mouse cardiomyocyte based on a previously reconstructed cardiac mitochondrial network (Vo et al. 2004) and a genome-scale metabolic model of *Mus musculus* (Sheikh et al. 2005). This network and isotopomer data from an isolated perfused mouse heart study (Khairallah et al. 2004) were used to estimate intracellular fluxes using the algorithm described in this paper.

Isotopomer data from the perfused mouse heart

The work of Khairallah et al. (2004) sought to characterize and trace the origin of pyruvate and citrate carbons in working mouse hearts. Four types of labeled substrates, perfused at their respective physiological concentrations, were used in the experiment; here we analyzed only the isotopomer data from the experiments with uniformly labeled glucose, [U-$^{13}C_6$] glucose, (50% initial enrichment).

In integrating these data into the model, we used three types of information. First, the reported molar enrichment of supplied glucose was used to set the isotopomer distribution of extracellular glucose.

Second, the upper and lower bounds on the uptake and efflux rates of lactate, pyruvate, glucose, citrate, succinate, oleate, oxygen set to two standard errors above and below the mean (Table 2). Third, the ^{13}C enrichment of CAC intermediates (citrate, α-ketoglutarate, succinate, fumarate, malate, oxaloacetate moiety of citrate) and their standard errors were used to formulate the objective function. These data were obtained from GC-MS, and the final enrichment, corrected for ^{13}C natural abundance, of each mass isotopomers was reported (Khairallah et al. 2004). We also used the average mouse heart wet weight to convert reported data into a consistent flux unit (μmol/min·gww).

Size and scope of the model

The present cardiomyocyte metabolic model accounts for 240 metabolites and 257 reactions, of which 39 are exchange reactions (Schilling et al. 2000). The rank of the corresponding stoichiometric matrix is 221. There are thus 36 reaction fluxes that have to be determined by using isotopomer data in addition to the mass-balance constraint. Reactions in this network describe glycolysis, the CAC, oxidative phosphorylation, ROS (reactive oxygen species) detoxification, anaplerosis, β-oxidation, ketone body metabolism, heme synthesis, and phospholipid synthesis. These reactions are written at the same level of detail as those in our previous reconstructed network (Vo et al. 2004). Contents of this network can be found in the supplemental data.

In using this model to analyze isotopomer data from the perfused mouse heart, we made four assumptions:

1) The 257 reactions included in the model are sufficient to describe the major metabolic activity in the perfused mouse heart.
2) The labeling of substrates with ^{13}C is assumed not to affect how they participate in a reaction, i.e. a metabolite is not selected against or preferred by an enzyme due to its labeling state.
3) The flux distribution that yields ^{13}C labeling patterns most resembling the observed isotopomers (of the isolated metabolites) is assumed to be the physiological flux distribution that the cell takes on.
4) The perfused mouse heart achieved a steady state during the course of the experiment.
5) There was labeling scrambling in reactions involving symmetric metabolites.

We tracked carbon transfer for 121 reactant-product pairs associated with 79 metabolites in the network. This translated to 1700 isotopomer variables. Carbons of the remaining metabolites were not tracked for one or more of three reasons: 1) the sizes of the metabolites are too large (long chain fatty

acids and heme); 2) the metabolites do not participate in carbon transfer reactions in the network (e.g. ATP and ADP); and 3) the metabolites are dead ends (Reed et al. 2003) in the networks. The IMMs for the 121 reaction-product pairs are available for download in MATLAB (The MathWorks, Inc., Natick, MA) matrix format at our group's website. We envision that a database of such IMMs can be a valuable repository of unambiguously defined reaction mechanisms. Note that a large number of these IMMs are identity matrices as most biochemical reactions do not involve carbon rearrangement. All identity IMMs were excluded from our isotopomer balance constraints to avoid unnecessary matrix computation.

Pyruvate branch points and fate

Pyruvate serves as an important branch point of substrate metabolism. It is thus useful to be able to quantify the contribution of various exogenous carbohydrate sources to tissue pyruvate. Cytosolic pyruvate was considered equivalent to tissue pyruvate for this purpose, as the mitochondrial pyruvate pool includes pyruvate produced by mitochondrial lactate dehydrogenase and malic enzyme. Based on the predicted fluxes for glucose uptake rate (3.00 ± 0.05 μmol/min·gww), pyruvate uptake rate (0.43 ± 0.06 μmol/min·gww), and lactate uptake rate (0.30 ± 0.05 μmol/min·gww), our estimated fractional contributions of these three exogenous substrates to cytosolic pyruvate were found to be 80 ± 2, 8 ± 2, and 12 ± 2% respectively (Appendix). Compared to the reported estimation by Khairallah et al. (2004) (Table 3), this estimate is rather different. We do not see this as a direct conflict as the earlier study used a different method of analysis. These authors used data from three experiments, each with a different labeled substrate, and computed the contributions based on the enrichment of M3 cytosolic pyruvate in each experiment. However, if they were to compute these fractional contributions using the estimated fluxes the uptake of glucose, pyruvate, and lactate reported in their study (Table 3), the result would be much closer to the values we report here (Appendix). These two methods are complementary in quantifying the contribution of exogenous carbohydrates to tissue pyruvate. The method by Khairallah et al. (2004) is more experimentally intensive, and may be affected by inconsistency and errors in these experiments. Such inconsistency is likely the reason that these authors could not account for the source that made up 26% of tissue pyruvate. On the other hand, our method is more computationally intensive, and does not account for the contribution of substrates other than exogenous glucose, lactate, and pyruvate.

Since tissue pyruvate was only enriched in M3 isotopomer, it was concluded that the pentose phosphate pathway activity was low. Therefore, the consumed ^{13}C glucose yielded a stoichiometric amount of glycolytic pyruvate at a rate of 3.00 ± 0.05 μmol/min·gww. Our model predicted that the

majority of cytosolic pyruvate was converted to lactate (90%), which in turn was excreted by the cell. This result agreed with the observed M3 lactate efflux rate when mouse hearts were perfused with [U $^{13}C_3$] pyruvate (Khairallah et al. 2004). The remaining pyruvate was transported into the mitochondria for further oxidation. Mitochondrial pyruvate had two major fates: oxidation by pyruvate dehydrogenase and anaplerosis by pyruvate carboxylase. Our estimated steady state rate for pyruvate dehydrogenase was 0.25 ± 0.00 μmol/min·gww, while that for pyruvate carboxylase was 0.02 ± 0.00. A small amount of mitochondrial pyruvate (15%) was also inter-converted with lactate via mitochondrial lactate dehydrogenase and the pyruvate-lactate shuttle.

Activities of the citric acid cycle

Citrate is produced from oxaloacetate and acetyl-CoA in every turn of the CAC. During the time course of the perfused experiment (20-30 min) (Khairallah et al. 2004), most of cellular energy was likely to be derived from substrates provided in the perfusate (glucose, pyruvate, lactate, and oleate). The contributions of amino acids from protein breakdown and lipid from membrane turnover were probably small, and hence not accounted for in our model. Therefore, the acetyl-CoA moiety of citrate (ac^{cit}) was derived from fatty acid or pyruvate decarboxylation, while the oxaloacetate moiety (oaa^{cit}) mostly came from pyruvate carboxylation. The origin of each citrate moiety was thus evaluated using the ratios of pyruvate decarboxylation and pyruvate carboxylation fluxes to that of citrate synthase. Based on the calculated fluxes for pyruvate dehydrogenase and pyruvate carboxylase, the pyruvate contribution to ac^{cit} and oaa^{cit} was estimated to be 17% and 1.4% of the CAC flux (1.51 ± 0.05 μmol/min·gww). In comparison, the CAC flux was previously estimated to be 1.88 ± 0.01 μmol/min·gww by Khairallah et al. (2004) assuming a linear relationship between oxygen consumption and citrate formation from carbohydrates and fats.

Recall that since the experimentally measured isotopomer distributions of the six CAC intermediates were used in the objective function, discrepancies observed in the calculated mass distribution vector (MDV) and the measured MDV (Figure 1) offer a good estimate of the accuracy of the flux calculation. We observed two key differences between the calculated and measured MDV. First, there was stronger agreement between the predicted and the experimental averages for M3 and M4 isotopomers, compared to M1 and M2, of the CAC intermediates. The experimental data for M3 and M4 isotopomers had more precise values (smaller standard errors), and thus the model favored flux distributions that had better fit for these isotopomers (see the Error function). The higher overall predicted ^{13}C enrichment for most CAC intermediates also indicated that there was a low level of ^{13}C

dilution (~10%) due to endogenous unlabeled carbon sources not accounted for in the model. Second, our results showed a decrease in total enrichment of α-ketoglutarate and succinate, reflecting the loss of ^{13}C to $^{13}CO_2$. On the other hand, the similar mass distributions calculated for succinate, fumarate, and malate were probably a consequence of i) fumarate being produced and consumed in the model only by succinate dehydrogenase and fumarase and ii) the rapid isotopomer randomization for symmetric metabolites in our assumption. Labeling data from Khairallah et al. (2004), however, did not have such a homogenous mass distributions for these three metabolites (Figure 1).

The CAC, together with oxidative phosphorylation, produces the majority of the ATP that is used for contractile function (Myosin ATPase) and various ion pumps in cardiomyocytes. We represented all ATP consuming reactions collectively as an ATP demand function, which described the hydrolysis of the high energy phosphate bond of ATP to ADP and pyrophosphate. This way, the ATP produced by metabolism of various substrate sources was coupled with an ATP consuming sink. The amount of ATP produced by anaerobic oxidation was 6.0 ± 0.1 μmol/min·gww, which was approximately 30% of the estimated total ATP production, 16.6 ± 2.3 μmol/min·gww. The total ATP production rate calculated based on isotopomer data using this model was less than 40% of the maximal ATP production rate computed based on respiration rate and substrate uptake rates alone (Vo et al. 2004).

Bidirectional reaction rates

Many enzymatic reactions are recognized to be bidirectional, i.e. reversible, as they operate near equilibrium in cellular physiological conditions. Even for reactions with low net fluxes, both forward and reverse rates can be quite high, rendering these rates unobservable during a typical experimental time scale. However, as both directions of the reactions affect the ^{13}C labeling patterns of reactants and products of the enzymes, it is possible to estimate these rates based on the isotopomers of these metabolites. In fact, one may incorrectly estimate the net flux of such reactions if the forward and reverse directions of the enzymes are ignored.

Of the 95 reversible reactions in the model, 55 reactions are associated with metabolites that have isotopomer tracking; these are the only reactions whose forward and reverse rates can be reliably estimated (supplemental data). The difference between the forward and the reverse rate, referred to as *exchange fluxes* (Wiechert and deGraaf 1997), were predicted with precision for 49 reactions (Note that the term exchange flux used here is not the same as *exchange reaction* (Schilling et al. 2000), which is used to describe metabolite crossing the system boundary). Histograms of these exchange fluxes (across

all the predicted locally optimal solutions) have dominant left peaks (supplemental data). Overall exchange fluxes are of the same order of magnitude as the net fluxes, but tend to be slightly lower than the values of net fluxes. The average net fluxes for the 49 reactions were found to be 0.46 μmol/min·gww, while the average exchange fluxes were 0.41.

Reversibility of reactions also provides information about the dynamics of flux patterns in a pathway. Seven out of ten reactions in the glycolytic pathway are considered reversible as they participate in both glycolysis and gluconeogenesis. However, as the heart does not have a high gluconeogenic activity, these reactions do not have high exchange fluxes; their exchange fluxes make up less than 50% of the net fluxes. The CAC has five reversible reactions; three of them (succinate dehydrogenase, malate dehydrogenase, and fumarase) have significantly higher exchange fluxes than the other two. The high exchange rates in these enzymes justify the isotopomer scrambling assumption in our model. Lastly, pseudoketogenesis, a process discovered by the label exchange between acetoacetate and acetoacetyl-CoA in rat hearts (Fink et al. 1988), is also observed in the exchange fluxes predicted by our model. The two reversible enzymes contributing to this pseudoketogenesis were found to have the following net and exchange fluxes: thiolase (0.72 and 0.24 μmol/min·gww), 3-ketoacyl-CoA transferase (0.41 and 0.13 μmol/min·gww). On the other hand, the net uptake to ketone bodies was found to be 0.27 (acetoacetate) and 0.46 (β-hydroxybutyrate) μmol/min·gww. Thus, pseudoketogeneis makes up as much as 50% the net ketone body uptake by the perfused mouse heart.

Properties of the predicted flux distributions

Reducing the solution space

Estimates for net and exchange fluxes for reactions in the network are shown in Table 4 and the supplemental data. We evaluated the amount of information gained by the addition of isotopomer data by comparing the estimated flux variation computed with and without the isotopomer balance constraints. The 149 reactions having no flux variation are not shown on Figure 2. Without isotopomer data, only about 20% of the remaining reactions (reactions with non-zero flux variation) could be predicted with reasonably small flux ranges. The application of isotopomer data, however, brought this number to 90%, a substantial improvement in flux estimation.

Sensitivity with respect to user-defined initial points

The locally optimal solutions returned by SNOPT were dependent on the user-defined starting points. Starting points computed by the linear programming method, v_{LP}^{net}, and by the Hit-and-Run algorithm (Kaufmann 1998; Thiele et al. 2005), v_{rand}^{net}, produced two sets of solutions, which we evaluated based on four characteristics: 1) success in finding locally optimal solutions with the starting points; 2) values of the objective function *Error*; 3) correlation of the best solution (solution yielding the smallest error) with other locally optimal solutions; and 4) range of flux variation of each reaction across locally optimal solutions found. First, the SNOPT solver was able to converge to locally optimal solutions for more than 80% of the initial points generated by the linear programming method, but only 50% with points generated by the Hit-and-Run algorithm. Second, the smallest errors found by both methods differed only by 0.1%. Comparing the two best solutions, found with v_{LP}^{net} and v_{rand}^{net} respectively, only 14 reactions have flux values differing by more than 5% from each other. Overall, approximately 90% of all locally optimal solutions found by the two methods had very similar error values (less than twice the error of the best solution); the remaining 10% were outliers with significantly higher errors (supplemental data).

Third, we limited our further analysis to only solutions with errors that were within 5% of the smallest error. This way, our predicted flux values provided the best estimates of the physiological fluxes without over fitting the measured mass distributions. Among this group of flux distributions, we determined that if two flux distributions were well correlated, then the individual reaction fluxes in the two distributions must be similar. As expected, SNOPT was more likely to converge to the same optimal solution for v_{LP}^{net} that maximizes or minimizes fluxes through reactions in the same pathways. In contrast, solutions found by v_{rand}^{net} were less correlated with one another, their correlation coefficient values ranged from 0.5 to 1 (supplemental data). Lower correlation among solutions found with the second method implied that there existed a number of reactions whose fluxes could not be determined precisely. The high correlations seen with the first method was likely a result of incomplete sampling of the solution space.

Lastly, in assessing how much the use of isotopomer data helped in determining reaction fluxes, we evaluated the range of each reaction flux for groups of flux distributions found with v_{LP}^{net} and with v_{rand}^{net}. Within the first group, 21 reactions had a standard deviation larger than 10% of the mean flux values. Among solutions in the second group, 28 reactions had the standard deviation larger than 10% the mean fluxes. The former 21 reactions were a subset of the latter 28 reactions, indicating that the second

initialization method provided a more exhaustive list of reactions whose fluxes could not be precisely determined by the isotopomer data. Taken together, these results point to the following conclusions. If one is only interested in the solution with the best objective value, it is possible to find such solution with either method of initialization. However, if one is interested in studying how a set of isotopomer data narrow the range of allowable flux values for each reaction, the second method of initialization provides a more thorough answer.

Sensitivity with respect to experimental error

In order to investigate the effects of the uncertainty associated with each isotopomer measurement on the results of the model, we generated random isotopomer measurements normally distributed with respect to the measurement statistics. These hypothetical measurements were used to evaluate how experimental errors affected the calculated flux distributions. The v_{rand}^{net} starting point yielding the best error value found in the previous study was used as the starting point here. The resulting solutions were also assessed based on the four characteristics mentioned above. A total of 98 out of the 100 sets of isotopomer data produced locally optimal solutions. Similar to the previous study, 90% of these solutions had very similar objective values, while the remaining 10% had significantly higher error values. The best flux distribution found from the previous sensitivity analysis, v^*, was as well correlated with solutions found with these hypothetical isotopomer data as it was with solutions found with the original dataset (supplemental data). In summary, we conclude that uncertainty associated with isotopomer measurement errors do not significantly change the estimated fluxes, so long as such uncertainty is sufficiently small (having similar relative errors as the data used here).

II) EFFECTS OF EXPERIMENTAL DESIGN

Choice of labeled carbon sources

In choosing the labeled substrates for an experiment, there are two considerations to keep in mind. First, the labeled substrates should lead to a high total ^{13}C enrichment in the cellular system after potential decarboxylation. Second, the labeled substrates should result in different mass distributions of isolated metabolites under different flux distributions. We investigated these two qualities by computing the isotopomer distributions of isolated metabolites (CAC intermediates) for a set of 1000 flux distributions. The 1000 flux distributions were calculated using the Hit-and-Run sampling algorithm (Kaufmann 1998; Thiele et al. 2005). We studied 12 commercially available substrate mixtures: **1)** 100%

[U-$^{13}C_6$] glucose; **2)** 100% [1 ^{13}C] glucose; **3)** 100% [2 ^{13}C] glucose; **4)** 100% [4 ^{13}C] glucose; **5)** 100% [6 ^{13}C] glucose; **6)** 50% [U-$^{13}C_6$] glucose and 50% [1,2 ^{13}C] glucose; **7)** 20% [U-$^{13}C_6$] glucose and 80% [1 ^{13}C] glucose; **8)** 20% [U-$^{13}C_6$] glucose and 80% [2 ^{13}C] glucose; **9)** 20% [U-$^{13}C_6$] glucose and 80% [3 ^{13}C] glucose; **10)** 20% [U-$^{13}C_6$] glucose and 80% [4 ^{13}C] glucose; **11)** 20% [U-$^{13}C_6$] glucose and 80% [5 ^{13}C] glucose; and **12)** 20% [U-$^{13}C_6$] glucose and 80% [6 ^{13}C] glucose. The seven mixtures producing substantially higher total enrichment of the CAC intermediates were 3, 4, 6, 8, 9, 10, and 11. In addition, we calculated the standard deviation for values of each mass isotopomer of each metabolite across the 1000 flux distributions. The substrate mixtures producing the largest overall standard deviations were 7, 9 and 10. Considering both qualities, we recommend using 20% [U-$^{13}C_6$] glucose and 80% [3 ^{13}C] glucose or 20% [U $^{13}C_6$] glucose and 80% [4 ^{13}C] glucose for studying CAC dynamics.

An isotopomer model generated under the framework described in this paper is based on the assumption that one can determine the isotopomer distribution of the products of a reaction if the reaction rate and the isotopomer distribution of reactant(s) are known. Therefore, it is essential that the isotopomer distribution of at least one metabolite is always known throughout the time course of the experiment. In practice, this can be done by supplying a tracer that is only taken up and not secreted by the cell at steady state. This way the isotopomer pool for that metabolite does not get "contaminated" by isotopomers that are produced by the cell. In the study by Khairallah *et al*. (2004), even though the perfusate was not recirculated after going through the heart, there is some mixing, in the extracellular space, of pyruvate supplied by the buffer and pyruvate produced by the cell. As a result, the isotopomer distribution of extracellular pyruvate was not known definitively through out the experiment. The same situation occurred in experiments with labeled lactate. Therefore, we concluded that of the four experiments by Khairallah *et al*. (2004), glucose and oleate are suitable substrates to be analyzed using the method described in this paper, but pyruvate and lactate are not.

Choice of flux or isotopomer measurement

In profiling metabolic fluxes, one can combine mass isotopomer data with flux measurements to accurately determine the intracellular flux distribution in a metabolic network. As flux measuring experiments tend to be intricate and difficult, it is useful to identify which reaction rates are the most informative for determining the rate of the remaining reactions. Based on the calculated flux distributions, we identified a set of 28 reactions, whose flux values could not be precisely determined with the present data. These reactions generally fall into two categories: ketone body and glutamine metabolism. Therefore, reaction fluxes or isotopomers of metabolites in pathways involving ketone

bodies and glutamine are good candidates for measurement in future experiments. By iteratively studying the results of previous measurements, each subsequent experiment benefits from the knowledge gained from previous experiments, and together they paint a more complete picture of the metabolic network.

DISCUSSION

In this study, we applied a computational method using isotopomer mapping matrices and the constraint-based framework to compute intracellular fluxes to analyze isotopomer data from perfused mouse hearts to highlight the advantages of this systemic approach in flux analysis. We used a rather large metabolic network to illustrate the scalability of the method and avoided simplifying reactions or merging metabolite pools so that a variety of examples for IMMs and isotopomer balance equations could be presented (http://systemsbiology.ucsd.edu/organisms/). From the predicted flux distribution, we determined fluxes at the pyruvate branch point, identified the origin of citrate, and estimated exchange fluxes of bidirectional reactions in glycolysis, the CAC and pseudoketogenesis.

The *ex vivo* perfusion experiment allowed the working mouse heart to take up four substrates ([U ^{13}C] glucose, pyruvate, lactate, and oleate) from a perfusate that was optimized to mimic physiological serum (Khairallah et al. 2004). At the respiration rate of 5.49 ± 0.06 μmol/min·gww, the heart was found to take up significantly higher (ten times) exogenous carbohydrates than the fatty acid oleate. After accounting for the efflux of pyruvate and lactate; however, oleate was found to have twice the amount of ATP contribution relative to glucose. Similar results were found by Khairallah et al. (2004), where the authors, using analytical expressions, reported a contribution of 62 ± 10% by fatty acids and 34 ± 4% by carbohydrates to the overall ATP production. Based on isotopomer data of the CAC intermediates, we predicted an average net flux of 1.51 ± 0.05 μmol/min·gww, a value very similar to that found in rat hearts, 1.7 ± 0.2 μmol/min·gww (Vincent et al. 2004). Anaplerosis by pyruvate carboxylation was found to be relatively small (amounts only to 1% of the CAC net flux), but, based on the difference between calculated and predicted isotopomer distributions, anaplerosis by endogenous substrate was estimated to be 10% of the CAC net flux. Finally, analysis of exchange fluxes showed psedoketogenesis can be a significant source of ketone bodies generated by the heart, amounting up to 50% of the overall ketone body uptake rate by the heart.

The optimization framework for predicting flux distribution from isotopomer data as described here produces a set of least-squares, best-fit, steady-state flux distributions from a given set of mass distribution data. For common metabolic networks, there is no guarantee of finding a globally optimal

solution in polynomial time. As a result, one must sample a sufficiently large group of local solutions, and identify a group of flux distributions that are the most likely physiological. Alternatively, one can select the solution with the least deviation from experimental data and designate that as the best and most probable flux distribution. The latter approach, however, is likely to over fit the data. Though the process of developing a comprehensive model as present here is more time consuming than deriving analytical expressions, the benefit of the approach is that once the network and associated constraints are set up, they can be applied to analyze isotopomer data for various tracers with very little modification. The AMMs and the IMMs are inherently modular; they only have to be constructed once and can be used in any networks that include the associated reactions. Isotopomer balance constraints can be automatically generated from the stoichiometric matrices and supplied IMMs. In addition, the constraint-based framework ensures that predictions made by the model can not contradict previously known information about reaction fluxes (those represented by constraints) and therefore the model can serve as a framework to resolve inconsistent data.

In applying this approach for isotopomer analysis, careful consideration must be taken to determine which experimental quantities can be set as constraints and which quantities are used to formulate the objective function. Constraints in the nonlinear programming problem specify mathematical relationships that the network must faithfully obey, while the objective function describes the preferable characteristics of the optimal solutions. Most studies, including this one, have used observed mass distribution data for the objective function, and measurements of substrate uptake and secretion rates as constraints. This practice is usually followed for two reasons. First, setting the mass distribution variables exactly equal to the mean of the observed data often eliminates all feasible steady states. In addition, including the standard deviations as the lower and upper bounds for these variables is cumbersome, and the resulting sum of elements of the isotopomer distribution vectors may not be unity. Second, it is much more straightforward to include flux means and standard deviations as constraints on reaction fluxes. The consequence of these constraints can be quickly determined by solving a linear programming problem that excludes the isotopomer balance constraints. Nevertheless, the decision on constraint formulation should be specific to the system of interest and confidence in the experimental measurements. We do, however, recommend setting sufficiently loose constraints to avoid eliminating physiologically relevant flux distributions.

In summary, we present here a method for flux analysis based on isotopomer data and demonstrate its usefulness in studying substrate metabolism in perfused mouse heart. All results discussed in this study are derived from the estimated flux values of all 257 reactions in the network

(Table 4), which are mutually consistent assuming that the reconstructed biochemical network (Supplemental data) is correct. Consequently, the validation (through comparison with published results from other studies) of a subset of reaction fluxes in our model also serves as an indirect validation for estimated fluxes of the remaining reactions, as all of these reactions are connected through a cohesive model representing the underlying biochemical network. In providing the model content and program source codes, it is our hope that future isotopomer studies will take advantage of the present computational methods so that results based on additional isotopomer data sets can be cross-validated with those reported here.

APPENDIX

Fractional pyruvate contribution

From glucose = (2*glucose uptake)/total fluxes producing cytosolic pyruvate

From pyruvate = pyruvate uptake/total fluxes producing cytosolic pyruvate

From lactate = lactate uptake/total fluxes producing cytosolic pyruvate

Total fluxes producing cytosolic pyruvate = 2*glucose uptake + pyruvate uptake + lactate uptake

ACKNOWLEDGMENTS

The authors would like to thank Drs. Steve van Dien, Anthony Burgard, Markus Herrgard, and Jennifer Reed for helpful discussions during this study. This research was partially supported by University of California Systemwide Biotechnology Research & Education Program GREAT Training Grant 2005-246 to T. D. V.

REFERENCES

Arauzo-Bravo MJ, Shimizu K. 2001. Estimation of bidirectional metabolic fluxes from MS and NMR data using positional representations. Genome Inform Ser Workshop Genome Inform 12:63-72.

Bederman IR, Reszko AE, Kasumov T, David F, Wasserman DH, Kelleher JK, Brunengraber H. 2004. Zonation of labeling of lipogenic acetyl-CoA across the liver: implications for studies of lipogenesis by mass isotopomer analysis. J Biol Chem 279(41):43207-16.

Christensen B, Gombert AK, Nielsen J. 2002. Analysis of flux estimates based on (13)C-labelling experiments. Eur J Biochem 269(11):2795-800.

Christensen B, Nielsen J. 2000. Metabolic network analysis of Penicillium chrysogenum using (13)C-labeled glucose. Biotechnol Bioeng 68(6):652-9.

Cohen DM, Bergman RN. 1997. Improved estimation of anaplerosis in heart using 13C NMR. Am J Physiol 273(6 Pt 1):E1228-42.

Comte B, Vincent G, Bouchard B, Des Rosiers C. 1997a. Probing the origin of acetyl-CoA and oxaloacetate entering the citric acid cycle from the 13C labeling of citrate released by perfused rat hearts. J Biol Chem 272(42):26117-24.

Comte B, Vincent G, Bouchard B, Jette M, Cordeau S, Rosiers CD. 1997b. A 13C mass isotopomer study of anaplerotic pyruvate carboxylation in perfused rat hearts. J Biol Chem 272(42):26125-31.

Dauner M, Bailey JE, Sauer U. 2001. Metabolic flux analysis with a comprehensive isotopomer model in Bacillus subtilis. Biotechnol Bioeng 76(2):144-56.

DeGrella RF, Light RJ. 1980. Uptake and metabolism of fatty acids by dispersed adult rat heart myocytes. I. Kinetics of homologous fatty acids. J Biol Chem 255(20):9731-8.

Fernandez CA, Des Rosiers C. 1995. Modeling of liver citric acid cycle and gluconeogenesis based on 13C mass isotopomer distribution analysis of intermediates. J Biol Chem 270(17):10037-42.

Fernandez CA, Des Rosiers C, Previs SF, David F, Brunengraber H. 1996. Correction of 13C mass isotopomer distributions for natural stable isotope abundance. J Mass Spectrom 31(3):255-62.

Fink G, Desrochers S, Des Rosiers C, Garneau M, David F, Daloze T, Landau BR, Brunengraber H. 1988. Pseudoketogenesis in the perfused rat heart. J Biol Chem 263(34):18036-42.

Fischer E, Sauer U. 2003. Metabolic flux profiling of Escherichia coli mutants in central carbon metabolism using GC-MS. Eur J Biochem 270(5):880-91.

Forbes NS, Clark DS, Blanch HW. 2001. Using isotopomer path tracing to quantify metabolic fluxes in pathway models containing reversible reactions. Biotechnol Bioeng 74(3):196-211.

Gill PE, Murray W, Saunders Ma. 2002. SNOPT: An SQP algorithm for large-scale constrained optimization. SIAM J. Optim 12(4):979-1006.

Gombert AK, Moreira dos Santos M, Christensen B, Nielsen J. 2001. Network identification and flux quantification in the central metabolism of Saccharomyces cerevisiae under different conditions of glucose repression. Journal of Bacteriology 183(4):1441-51.

Haymond MW, Sunehag AL. 2000. The reciprocal pool model for the measurement of gluconeogenesis by use of [U-(13)C]glucose. Am J Physiol Endocrinol Metab 278(1):E140-5.

Katz J, Lee WN, Wals PA, Bergner EA. 1989. Studies of glycogen synthesis and the Krebs cycle by mass isotopomer analysis with [U-13C]glucose in rats. J Biol Chem 264(22):12994-3004.

Katz J, Tayek JA. 1999. Recycling of glucose and determination of the Cori Cycle and gluconeogenesis. Am J Physiol 277(3 Pt 1):E401-7.

Kaufmann DE, Smith, R.L. 1998. Direction Choice for Accelerated Convergence in Hit-and-Run Sampling. Operations Research 46:84-95.

Khairallah M, Labarthe F, Bouchard B, Danialou G, Petrof BJ, Des Rosiers C. 2004. Profiling substrate fluxes in the isolated working mouse heart using 13C-labeled substrates: focusing on the origin and fate of pyruvate and citrate carbons. Am J Physiol Heart Circ Physiol 286(4):H1461-70.

Klapa MI, Aon JC, Stephanopoulos G. 2003. Systematic quantification of complex metabolic flux networks using stable isotopes and mass spectrometry. European Journal of Biochemistry 270(17):3525-3542.

Klapa MI, Park SM, Sinskey AJ, Stephanopoulos G. 1999. Metabolite and isotopomer balancing in the analysis of metabolic cycles: I. Theory. Biotechnol Bioeng 62(4):375-391.

Malloy CR, Jones JG, Jeffrey FM, Jessen ME, Sherry AD. 1996. Contribution of various substrates to total citric acid cycle flux and anaplerosis as determined by 13C isotopomer analysis and O2 consumption in the heart. Magma 4(1):35-46.

Marx A, deGraaf AA, Wiechert W, Eggeling L, Sahm H. 1996. Determination of the fluxes in the central metabolism of Corynebacterium glutamicum by nuclear magnetic resonance spectroscopy combined with metabolite balancing. Biotechnology and Bioengineering 49(2):111-129.

Nielsen J. 2003. It is all about metabolic fluxes. J Bacteriol 185(24):7031-5.

Panchal AR, Comte B, Huang H, Kerwin T, Darvish A, des Rosiers C, Brunengraber H, Stanley WC. 2000. Partitioning of pyruvate between oxidation and anaplerosis in swine hearts. Am J Physiol Heart Circ Physiol 279(5):H2390-8.

Puchowicz MA, Bederman IR, Comte B, Yang D, David F, Stone E, Jabbour K, Wasserman DH, Brunengraber H. 1999. Zonation of acetate labeling across the liver: implications for studies of lipogenesis by MIDA. Am J Physiol 277(6 Pt 1):E1022-7.

Reed JL, Famili I, Thiele I, Palsson BO. 2006. Towards multidimensional genome annotation. Nat Rev Genet 7(2):130-41.

Reed JL, Vo TD, Schilling CH, Palsson BO. 2003. An expanded genome-scale model of Escherichia coli K-12 (iJR904 GSM/GPR). Genome Biol 4(9):R54.

Schilling CH, Letscher D, Palsson BO. 2000. Theory for the systemic definition of metabolic pathways and their use in interpreting metabolic function from a pathway-oriented perspective. J Theor Biol 203(3):229-48.

Schmidt K, Carlsen M, Nielsen J, Villadsen J. 1997. Modeling isotopomer distributions in biochemical networks using isotopomer mapping matrices. Biotechnology and Bioengineering 55(6):831-840.

Schmidt K, Marx A, de Graaf AA, Wiechert W, Sahm H, Nielsen J, Villadsen J. 1998. C-13 tracer experiments and metabolite balancing for metabolic flux analysis: Comparing two approaches. Biotechnology and Bioengineering 58(2-3):254-257.

Schmidt K, Nielsen J, Villadsen J. 1999. Quantitative analysis of metabolic fluxes in Escherichia coli, using two-dimensional NMR spectroscopy and complete isotopomer models. J Biotechnol 71(1-3):175-89.

Sheikh K, Forster J, Nielsen LK. 2005. Modeling hybridoma cell metabolism using a generic genome-scale metabolic model of Mus musculus. Biotechnol Prog 21(1):112-21.

Sherry AD, Jeffrey FM, Malloy CR. 2004. Analytical solutions for (13)C isotopomer analysis of complex metabolic conditions: substrate oxidation, multiple pyruvate cycles, and gluconeogenesis. Metab Eng 6(1):12-24.

Thiele I, Price ND, Vo TD, Palsson BO. 2005. Candidate metabolic network states in human mitochondria. Impact of diabetes, ischemia, and diet. J Biol Chem 280(12):11683-95.

Van Dien SJ, Strovas T, Lidstrom ME. 2003. Quantification of central metabolic fluxes in the facultative methylotroph methylobacterium extorquens AM1 using 13C-label tracing and mass spectrometry. Biotechnol Bioeng 84(1):45-55.

van Winden WA, Heijnen JJ, Verheijen PJ. 2002. Cumulative bondomers: a new concept in flux analysis from 2D [13C,1H] COSY NMR data. Biotechnol Bioeng 80(7):731-45.

van Winden WA, van Gulik WM, Schipper D, Verheijen PJ, Krabben P, Vinke JL, Heijnen JJ. 2003. Metabolic flux and metabolic network analysis of Penicillium chrysogenum using 2D [13C, 1H] COSY NMR measurements and cumulative bondomer simulation. Biotechnol Bioeng 83(1):75-92.

Vincent G, Bouchard B, Khairallah M, Des Rosiers C. 2004. Differential modulation of citrate synthesis and release by fatty acids in perfused working rat hearts. Am J Physiol Heart Circ Physiol 286(1):H257-66.

Vo TD, Greenberg HJ, Palsson BO. 2004. Reconstruction and functional characterization of the human mitochondrial metabolic network based on proteomic and biochemical data. J Biol Chem 279(38):39532-40.

Wiechert W, deGraaf AA. 1997. Bidirectional reaction steps in metabolic networks .1. Modeling and simulation of carbon isotope labeling experiments. Biotechnology and Bioengineering 55(1):101-117.

Wiechert W, Mollney M, Isermann N, Wurzel M, de Graaf AA. 1999. Bidirectional reaction steps in metabolic networks: III. Explicit solution and analysis of isotopomer labeling systems. Biotechnol Bioeng 66(2):69-85.

Wiechert W, Siefke C, deGraaf AA, Marx A. 1997. Bidirectional reaction steps in metabolic networks .2. Flux estimation and statistical analysis. Biotechnology and Bioengineering 55(1):118-135.

Wittmann C, Heinzle E. 1999. Mass spectrometry for metabolic flux analysis. Biotechnology and Bioengineering 62(6):739-750.

Yarmush M, Berthiaume F. 1997. Metabolic engineering and human disease. Nature Biotechnology 15(6):525-528.

Zupke C, Stephanopoulos G. 1994. Modeling of Isotope Distributions and Intracellular Fluxes in Metabolic Networks Using Atom Mapping Matrices. Biotechnology Progress 10(5):489-498.

FIGURES

Figure 1: **Predicted (calculated) mass distributions for CAC intermediates as compared to experimentally measured mass distribution**. In each panel, values from left to right are M4, M3, M2, and M1, reported as average molar percent enrichment. The error bars are SE associated with experimental data reported by Khairallah et al. (2004). Predicted mass distributions also have associated standard deviations, but such deviations are very small and are not visible in the figure. Compared to M1 and M2 isotopomers, there is stronger agreement between the predicted and the experimental averages for M3 and M4 isotopomers of the CAC intermediates. The experimental data for M3 and M4 isotopomers have smaller standard errors, and thus the model favors flux distributions that have better fit for these isotopomers. Oaa(cit) refers to the oxaloacetate moiety of citrate.

Figure 2: **Estimated flux variation from the non-linear model using isotopomer data as compared to those from the linear model not using isotopomer data**. "All locally optimal solutions with isotopomer data" refers to all solutions that the SNOPT solver returns with "locally optimal" status. Some of these solutions may have very large error values. "Locally optimal solutions with smallest Error" refers to solutions with objective values no more than 5% of the smallest error found. The precision in flux estimation is at least one order of magnitude better when isotopomer data are used (Figure 2a). Flux variations have the unit of μmol/min·gww. A total of 149 reactions (not shown) have constant flux values. Flux variation is also reduced if one considers only flux distributions with the smallest errors rather than all locally optimal solutions (Figure 2b) returned by the solver.

TABLES

Table 1: Procedures to develop a constraint-based model for intracellular flux estimation based on reaction stoichiometry, substrate uptake and efflux rates, and isotopomer data. Detailed descriptions of each step are provided in the text and cited references

Step 1. Construct a stoichiometric matrix **S** representing the biochemical reactions in the network

Step 2. Construct atom and isotopomer mapping matrices

A. Identify metabolites that have carbon tracking, note symmetric metabolites
B. Construct AMM for reactant-product pairs of metabolites in step A
C. Compute IMM for each AMM

Step 3. Formulate constraints

A. Linear constraints:

$$\mathbf{S} \cdot v^{net} = 0$$

S is the stoichiometric matrix; v^{net} is a vector of unknown net fluxes

For all irreversible reactions *i*

$$\alpha_i \le v^{net} \le \beta_i$$

α_i and β_i represent the lower and upper bounds on the steady state reaction rates

For all reversible reactions *j*

$$v_j^{net} = v_j^{forward} - v_j^{reverse}$$

$$\alpha_j \le v^{net} \le \beta_j; 0 \le v^{forward} \le |\beta_j|;\ 0 \le v^{reverse} \le |\alpha_j|$$

For all metabolites *k* with carbon tracking; *C* is the number of carbon atoms in metabolite *k*.

$$\sum_{i=1}^{C(k)} IDV_i^k = 1$$

B. Nonlinear constraints: isotopomer balance equations

$$F_k(IDV_i^k, v) = 0$$

where the function F_k for each metabolite *k* is defined in Schmidt et al. 1997

Step 4. Solve for optimal flux distributions

A. Pick an initial starting v_o satisfying $\mathbf{S} \cdot v^{net} = 0$
B. Solve

$$Min \quad Error = \left(\sum_i^M \sum_j^{N(i)} \left(\frac{MDV_{i,j}^{measured} - MDV_{i,j}^{calculated}}{\sigma_{i,j}} \right)^2 \right)^{1/2}$$

Subject to Constraints 3A-3B.

$MDV_{i,j}$: mole fraction of mass isotopomer *j* of metabolite *i*
$\sigma_{i,j}$: standard deviation associated with that measurement $MDV_{i,j}$
N(*i*) : total number of mass isotopomers of metabolite *i*
M : number of metabolites measured in the experiment.

C. Repeat 4A-4B for a sufficiently large number of flux distributions

Table 2: Constraints on substrate uptake and efflux. The constraints for oxygen, pyruvate, lactate, citrate, and succinate were converted directly from flux values reported by Khairallah et al. (2004) in the experiments with [U-$^{13}C_6$] glucose. We interpreted the reported unit of μmol/min as μmol/min·heart, and used the reported mouse heart wet weight to convert this unit to μmol/min·gww. These constraints were set at two SE around the mean. These values represent only the **net** uptake (negative) or secretion (positive) by the cells. Pyruvate and lactate are allowed to be simultaneously taken up and released by the cells, as observed in the experiment. The positive upper and lower bounds specify a net secretion of these two metabolites. All numbers were derived from Khairallah *et al.* except for oleate which was taken from DeGrella and Light (1980) and the lower bound for glucose, which was set arbitrary large.

Substrates	Lower bound	Upper bound
Glucose	-10.00	-1.455
Lactate	1.33	2.17
Pyruvate	0.125	0.625
Oleate	-0.30	0.00
Citrate	0.015	0.019
Succinate	0.005	0.017
Oxygen	-7.05	-5.45

Table 3: Fractional contribution of exogenous carbohydrates to cytosolic pyruvate. Fractional contribution of each exogenous carbohydrate was calculated based on reaction fluxes calculated in the model (Appendix). Estimated values for Khairallah et al. (2004) were computed using flux results reported in that paper, with pyruvate uptake = 0.11 ± 0.02 μmol/min, lactate uptake = 0.09 ± 0.03 μmol/min, and glucose uptake rate > 0.51 ± 0.06 μmol/min (sum of lactate and pyruvate efflux when the heart was perfused with [U $^{13}C_6$] glucose). Values are reported as mean ± SD for this study and mean ± SE for Khairallah *et al.*

	Fractional contribution (%)	
	This study	Khairallah et al.
Glucose	80 ± 2	> 72 ± 8
Lactate	8 ± 2	< 15 ± 4
Pyruvate	12 ± 2	< 13 ± 3

Table 4: Estimated net and exchange fluxes (EXCH) as predicted by the model using isotopomer data. Net fluxes are reported as mean ± SD μmol/min·gww. SD values were computed across all locally optimal solutions with objective values no more than 5% larger than the smallest error found. Only reactions with non-zero net fluxes are shown here. Negative net fluxes mean that the fluxes flow in the reverse direction. Symbols [c], [e], and [m] stand for cytosolic, extracellular, and mitochondrial localization. FA oxidation: fatty acid oxidation, OxPhos: oxidative phosphorylation, ROS: reactive oxygen species detoxification, CAC: citric acid cycle, Mito transport: mitochondrial transport, NTR: exchange fluxes not tracked for reason described in the paper.

NAME	EQUATION	PATHWAY	MEAN	SD	EXCH
GLNS	[c] : atp + glu-L + nh4 --> adp + gln-L + h + pi	Amino acid	5.40	5.98	
GLUNm	[m] : gln-L + h2o --> glu-L + nh4	Amino acid	5.40	5.98	
LDH_L	[c] : lac-L + nad <==> h + nadh + pyr	Anaplerosis	-1.89	0.26	0.11
LDH_Lm	[m] : lac-L + nad <==> h + nadh + pyr	Anaplerosis	-0.21	0.25	0.03
PCm	[m] : atp + hco3 + pyr --> adp + h + oaa + pi	Anaplerosis	0.02	0.00	
FAOXC160	[m] : (7) coa + (7) fad + (7) h2o + (7) nad + pmtcoa --> (8) accoa + (7) fadh2 + (7) h + (7) nadh	FA oxidation	0.30	0.00	
FAOXC181	[m] : coa + h2o + nad + odecoa --> accoa + h + nadh + pmtcoa	FA oxidation	0.30	0.00	
CRNtim	crn[m] --> crn[c]	FA oxidation	0.30	0.00	
C181CPT1	[c] : crn + odecoa --> coa + odecrn	FA oxidation	0.30	0.00	
C181CRNt	odecrn[c] --> odecrn[m]	FA oxidation	0.30	0.00	
C181CPT2	[m] : coa + odecrn --> crn + odecoa	FA oxidation	0.30	0.00	
FACOAL181i	[c] : atp + coa + ocdcea --> amp + odecoa + ppi	FA oxidation	0.30	0.00	
HEX1	[c] : atp + glc-D --> adp + g6p + h	Glycolysis	1.50	0.03	
PGI	[c] : g6p <==> f6p	Glycolysis	1.50	0.03	0.77
PFK	[c] : atp + f6p --> adp + fdp + h	Glycolysis	1.50	0.03	
FBA	[c] : fdp <==> dhap + g3p	Glycolysis	1.50	0.03	0.35
TPI	[c] : dhap <==> g3p	Glycolysis	1.50	0.03	0.77
GAPD	[c] : g3p + nad + pi <==> 13dpg + h + nadh	Glycolysis	3.00	0.05	1.37
PGK	[c] : 3pg + atp <==> 13dpg + adp	Glycolysis	-3.00	0.05	1.22
PGM	[c] : 2pg <==> 3pg	Glycolysis	-3.00	0.05	1.39
ENO	[c] : 2pg <==> h2o + pep	Glycolysis	3.00	0.05	1.43
PYK	[c] : adp + h + pep --> atp + pyr	Glycolysis	3.00	0.05	
ACACT1rm	[m] : (2) accoa <==> aacoa + coa	Ketone bodies	0.72	0.03	0.24
HMGCOASim	[m] : aacoa + accoa + h2o --> coa + h + hmgcoa	Ketone bodies	1.13	0.92	
HMGLm	[m] : hmgcoa --> acac + accoa	Ketone bodies	1.13	0.92	
BDHm	[m] : bhb + nad <==> acac + h + nadh	Ketone bodies	-0.46	0.33	0.50
OCOAT1m	[m] : acac + succoa <==> aacoa + succ	Ketone bodies	0.41	0.91	0.13
ACCOACm	[m] : accoa + atp + hco3 --> adp + h + malcoa + pi	Lipid	4.50	4.60	
MCD	[m] : h + malcoa --> accoa + co2	Lipid	4.50	4.60	
ASPGLUm	asp-L[m] + glu-L[c] + h[c] <==> asp-L[c] + glu-L[m] + h[m]	Mal-Asp Shuttle	1.11	0.25	1.30
ASPTA	[c] : akg + asp-L <==> glu-L + oaa	Mal-Asp Shuttle	1.11	0.25	1.14
MDH	[c] : mal-L + nad <==> h + nadh + oaa	Mal-Asp Shuttle	-1.11	0.25	1.01
AKGMALtm	akg[m] + mal-L[c] <==> akg[c] + mal-L[m]	Mal-Asp Shuttle	1.11	0.25	2.02
ASPTAm	[m] : akg + asp-L <==> glu-L + oaa	Mal-Asp Shuttle	-1.11	0.25	1.02
ADK1	[c] : amp + atp <==> (2) adp	Nucleotide	0.30	0.00	NTR
NDPK1	[c] : atp + gdp <==> adp + gtp	Nucleotide	-1.08	0.92	NTR
HCO3Em	[m] : co2 + h2o <==> h + hco3	Others	4.52	4.60	1.02
PPA	[c] : h2o + ppi --> h + (2) pi	Others	0.30	0.00	
NADH2-u10m	(5) h[m] + nadh[m] + q10[m] --> (4) h[c] + nad[m] + q10h2[m]	OxPhos	7.56	0.18	
SUCD3-u10m	[m] : fadh2 + q10 <==> fad + q10h2	OxPhos	3.59	0.05	NTR
CYOR-u10m	(2) ficytC[m] + (2) h[m] + q10h2[m] --> (2) focytC[m] + (4) h[c] + q10[m]	OxPhos	11.15	0.13	
CYOOm3	(4) focytC[m] + (7.92) h[m] + o2[m] --> (4) ficytC[m] + (4) h[c] + (1.96) h2o[m] + (0.02) o2-[m]	OxPhos	5.58	0.06	
ATPS4m	adp[m] + (4) h[c] + pi[m] --> atp[m] + (3) h[m] + h2o[m]	OxPhos	23.08	3.94	
SPODMm	[m] : (2) h + (2) o2- --> h2o2 + o2	ROS	0.06	0.00	
CATm	[m] : (2) h2o2 --> (2) h2o + o2	ROS	0.03	0.01	
PDHm	[m] : coa + nad + pyr --> accoa + co2 + nadh	CAC	0.25	0.00	
CSm	[m] : accoa + h2o + oaa --> cit + coa + h	CAC	1.51	0.05	
ACONTm	[m] : cit <==> icit	CAC	1.49	0.05	0.17
ICDHxm	[m] : icit + nad --> akg + co2 + nadh	CAC	1.49	0.05	
AKGDm	[m] : akg + coa + nad --> co2 + nadh + succoa	CAC	1.49	0.05	

SUCOAS1m	[m] : coa + gtp + succ <==> gdp + pi + succoa	CAC	-1.08	0.92	0.04
SUCD1m	[m] : fad + succ <==> fadh2 + fum	CAC	1.49	0.05	20.41
FUMm	[m] : fum + h2o <==> mal-L	CAC	1.49	0.05	21.62
MDHm	[m] : mal-L + nad <==> h + nadh + oaa	CAC	2.60	0.23	46.10
CITt4	cit[e] <==> cit[c]	Transport	-0.02	0.00	0.01
GLCt1	glc-D[e] --> glc-D[c]	Transport	1.50	0.03	
L-LACt2r	h[e] + lac-L[e] <==> h[c] + lac-L[c]	Transport	-2.10	0.05	0.30
PYRt2r	h[e] + pyr[e] <==> h[c] + pyr[c]	Transport	-0.62	0.00	0.43
OCDCEAt	ocdcea[e] --> ocdcea[c]	Transport	0.30	0.00	
ACACt2	acac[e] + h[e] <==> acac[c] + h[c]	Transport	-0.27	0.36	0.03
BHBt	bhb[e] + h[e] <==> bhb[c] + h[c]	Transport	-0.46	0.33	0.35
Ht	h[c] <==> h[e]	Transport	0.09	0.00	NTR
CO2t	co2[e] <==> co2[c]	Transport	-3.22	0.10	0.84
H2Ot	h2o[e] <==> h2o[c]	Transport	-3.68	0.25	NTR
O2t	o2[e] <==> o2[c]	Transport	5.49	0.06	NTR
GLNtm	gln-L[c] --> gln-L[m]	Mito transport	5.40	5.98	
GLUt2m	glu-L[c] + h[c] <==> glu-L[m] + h[m]	Mito transport	-5.40	5.98	0.35
CITtam	cit[c] + mal-L[m] <==> cit[m] + mal-L[c]	Mito transport	-0.02	0.00	0.07
L-LACtm	h[c] + lac-L[c] <==> h[m] + lac-L[m]	Mito transport	-0.21	0.25	0.03
MALtm	mal-L[c] + pi[m] <==> mal-L[m] + pi[c]	Mito transport	-0.02	0.00	0.07
PYRt2m	h[c] + pyr[c] <==> h[m] + pyr[m]	Mito transport	0.49	0.25	0.33
CO2tm	co2[c] <==> co2[m]	Mito transport	-3.22	0.10	0.77
H2Otm	h2o[c] <==> h2o[m]	Mito transport	-17.61	2.38	NTR
Htm	h[c] --> h[m]	Mito transport	8.78	12.95	
NH4tm	nh4[c] <==> nh4[m]	Mito transport	-5.40	5.98	NTR
O2tm	o2[c] <==> o2[m]	Mito transport	5.49	0.06	NTR
PIt2m	h[c] + pi[c] <==> h[m] + pi[m]	Mito transport	19.61	6.04	NTR
ACACtm2	acac[c] + h[c] <==> acac[m] + h[m]	Mito transport	-0.27	0.36	0.04
BHBtm	bhb[c] + h[c] <==> bhb[m] + h[m]	Mito transport	-0.46	0.33	0.32
ATPtm	adp[c] + atp[m] --> adp[m] + atp[c]	Mito transport	18.55	5.99	
GTPtm	gdp[c] + gtp[m] --> gdp[m] + gtp[c]	Mito transport	1.08	0.92	

Figure 1

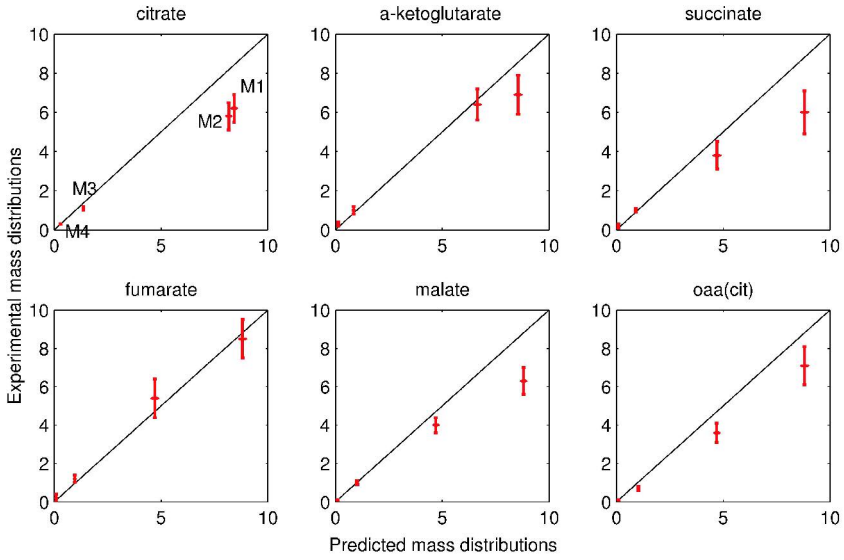

Figure 2a

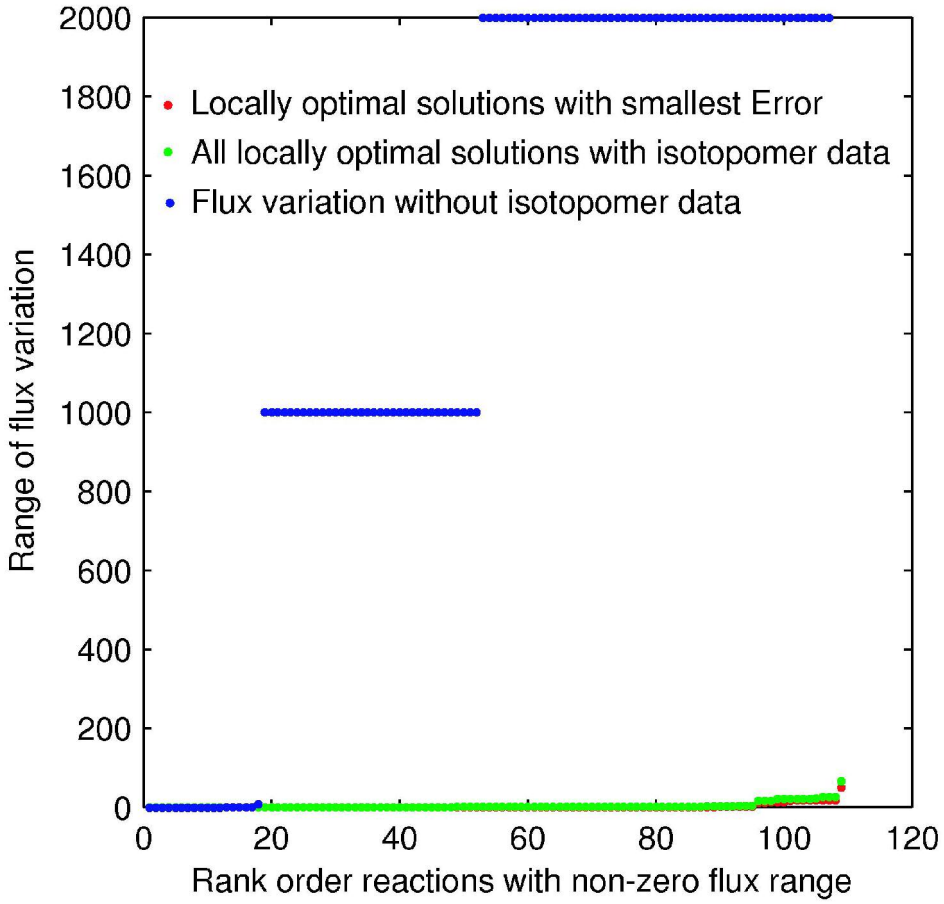
Locally optimal solutions with smallest Error
All locally optimal solutions with isotopomer data
Flux variation without isotopomer data
Range of flux variation
Rank order reactions with non-zero flux range
0
200
400
600
800
1000
1200
1400
1600
1800
2000
0
20
40
60
80
100
120

Figure 2b

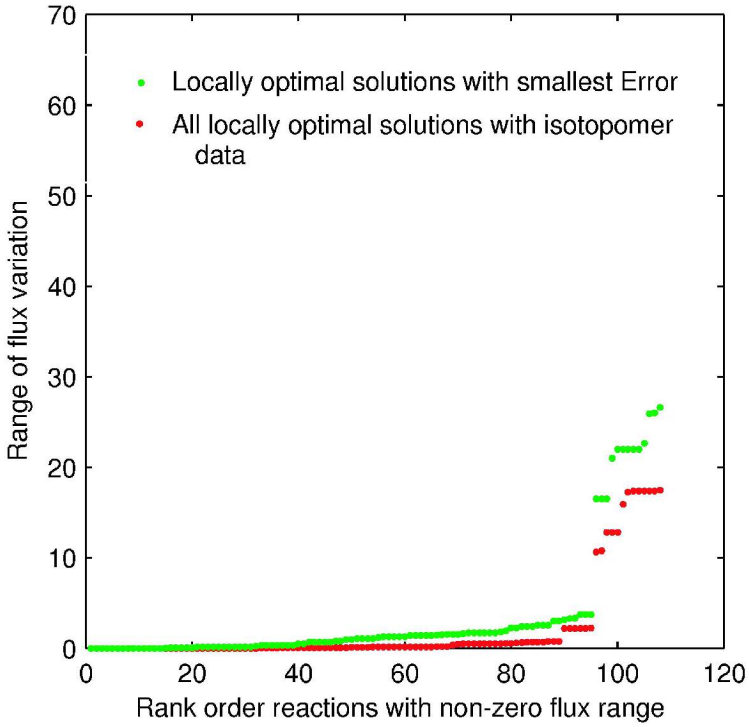

SUPPLEMETNAL DATA S1: Results from sensitivity analysis

Figure 1: Linear programming (LP) methods were used to define initial points, from which we computed locally optimal solutions (using the SNOPT solver in GAMS) below. Panel **A** shows the error values (values of the objective function) of all solutions returned with "locally optimal status" by the solver. Every blue dot represents the error of the flux distribution marked on x-axis. As shown, more than 90% of these solutions have very similar error values, the remaining has significantly higher. Every open circle (green) indicates the correlation between the first flux distribution (smallest error) and the flux distribution marked on the x-axis. Panel **B** is similar to panel A, except that only solutions within 5% error of the best solution (smallest error) are shown.

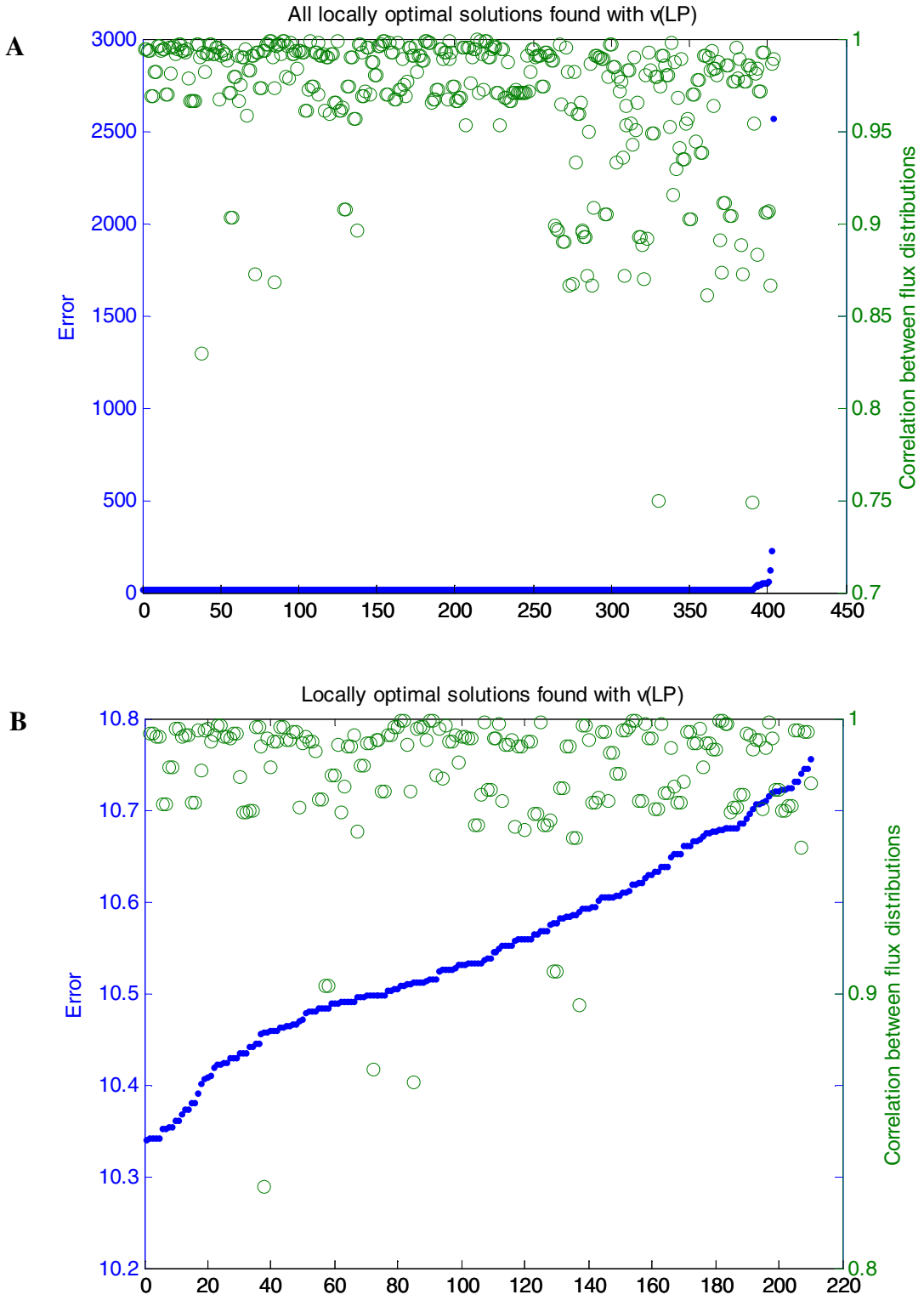

Figure 2: The Hit-and-Run random sampling algorithm was used to define initial points, from which we computed locally optimal solutions (using the SNOPT solver in GAMS) below. Panel **A** shows the error values (values of the objective function) of all solutions returned with "locally optimal" status by the solver. Every blue dot represents the error of the flux distribution marked on x-axis. As shown, more than 90% of these solutions have very similar error values, the remaining has significantly higher. Every open circle (green) indicates the correlation between the first flux distribution (smallest error) and the flux distribution marked on the x-axis. Panel **B** is similar to panel A, except that only solutions within 5% error of the best solution (smallest error) are shown.

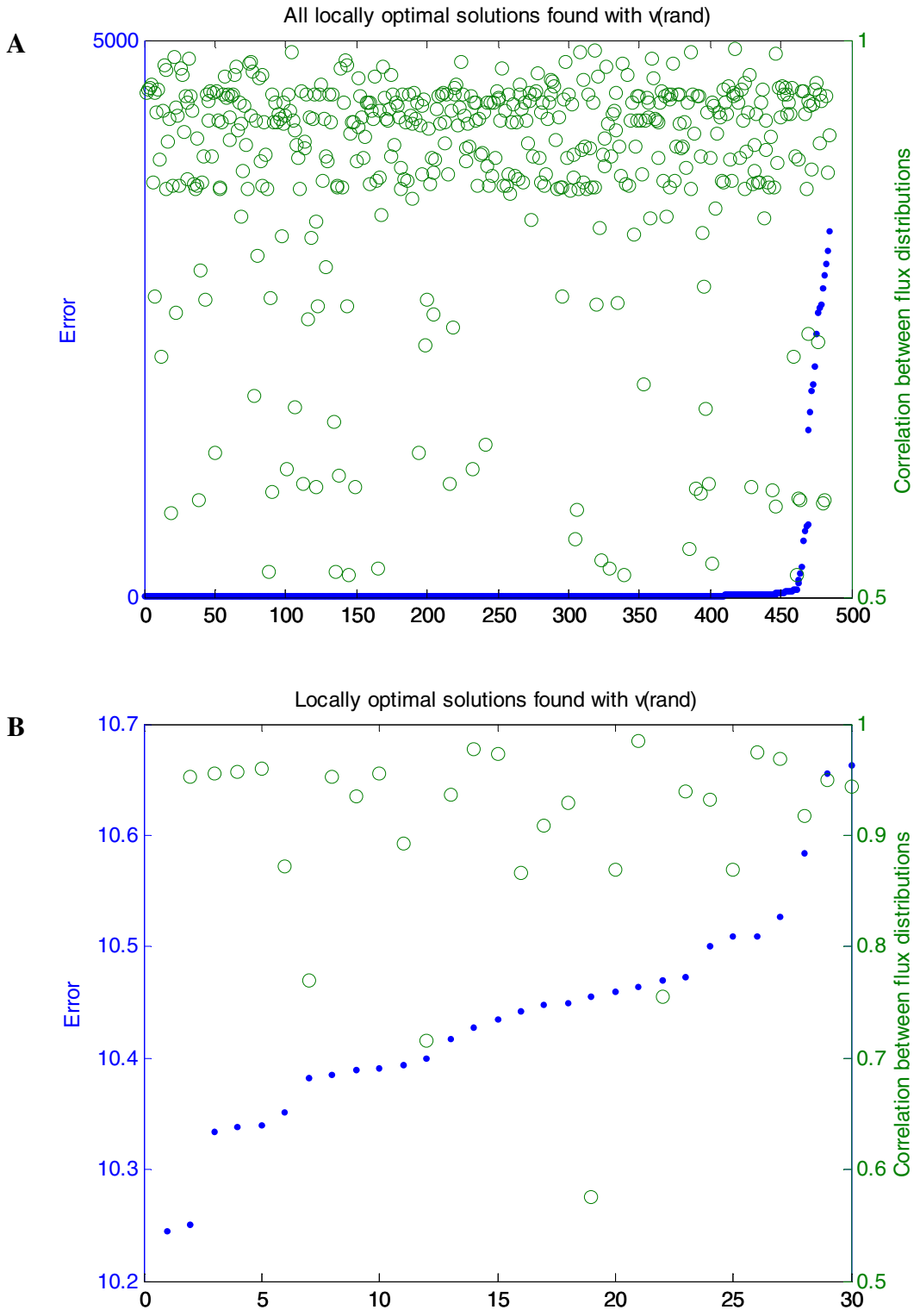

Figure 3: A normal distribution of isotopomer data based on reported mean and SE was created for each isotopomers of each isolated metabolite (citric acid cycle intermediates). From these distributions, we randomly drew values to make 100 hypothetical isotopomer datasets, and computed for resulting flux distributions. Panel **A** shows the error values of all solutions returned with "locally optimal" status by the solver. Every blue dot represents the error of the flux distribution marked on x-axis. Every open circle (green) indicates the correlation between the flux distribution marked on the x-axis and the best flux distribution found with the original data (data point 1, Figure 2B). Panel **B** is similar to panel A, except that only solutions within 5% error of the best solution (smallest error) are shown.

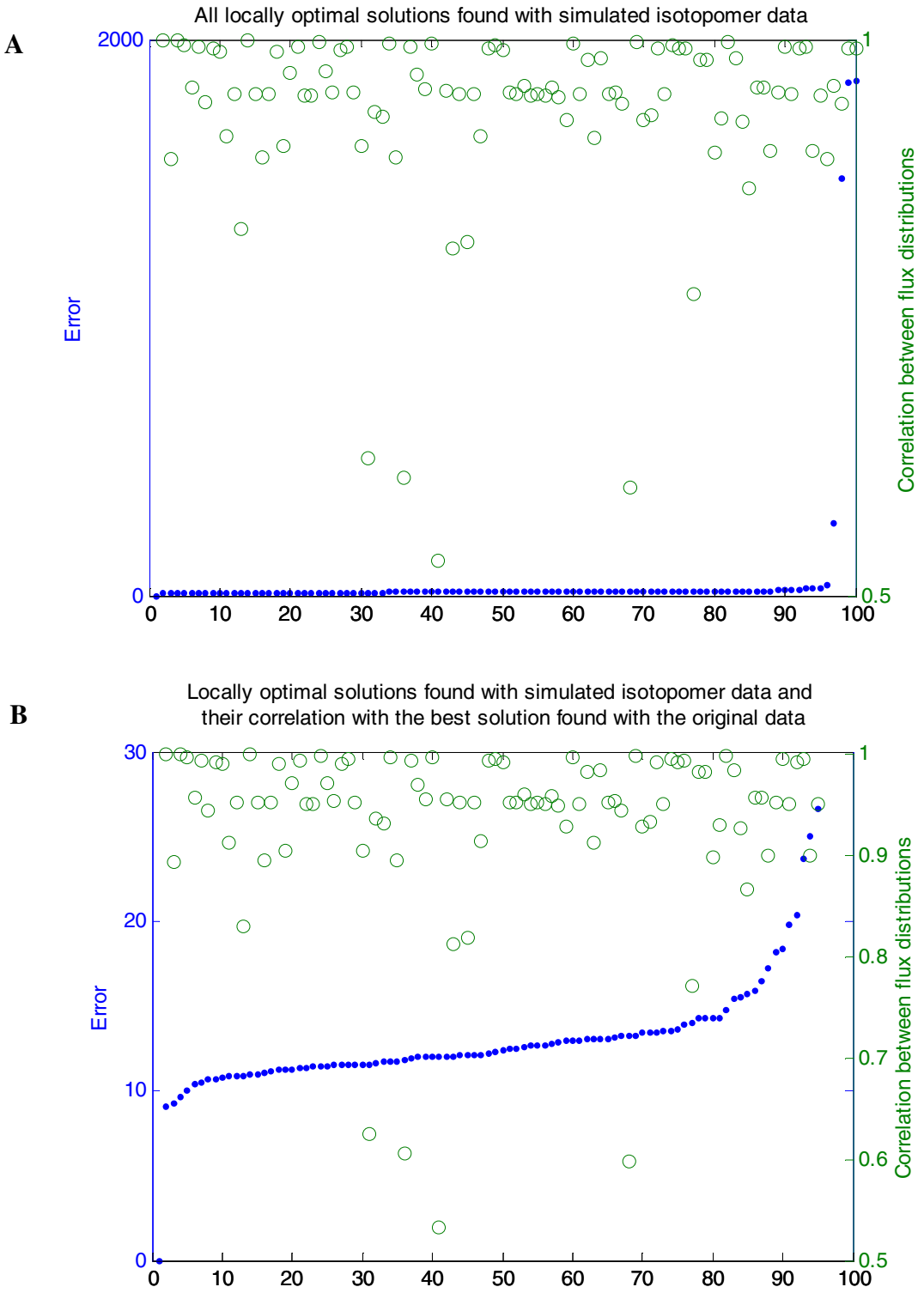

SUPPLEMENTAL DATA S2:

Histogram of exchange fluxes for bidirectional reactions in the network

See reaction list (Supplemental data S3) for reaction definitions. Exchange fluxes shown here are taken from the 30 flux distributions that have the smallest Error (difference between the observed and calculated mass isotopomer data); thus each of the below histogram contains 30 data points. Six reactions with the highest and most variable exchange fluxes are ASPMALm, FUMm, GLUDxm, GLUDym, MDHm, and SUCD1m.

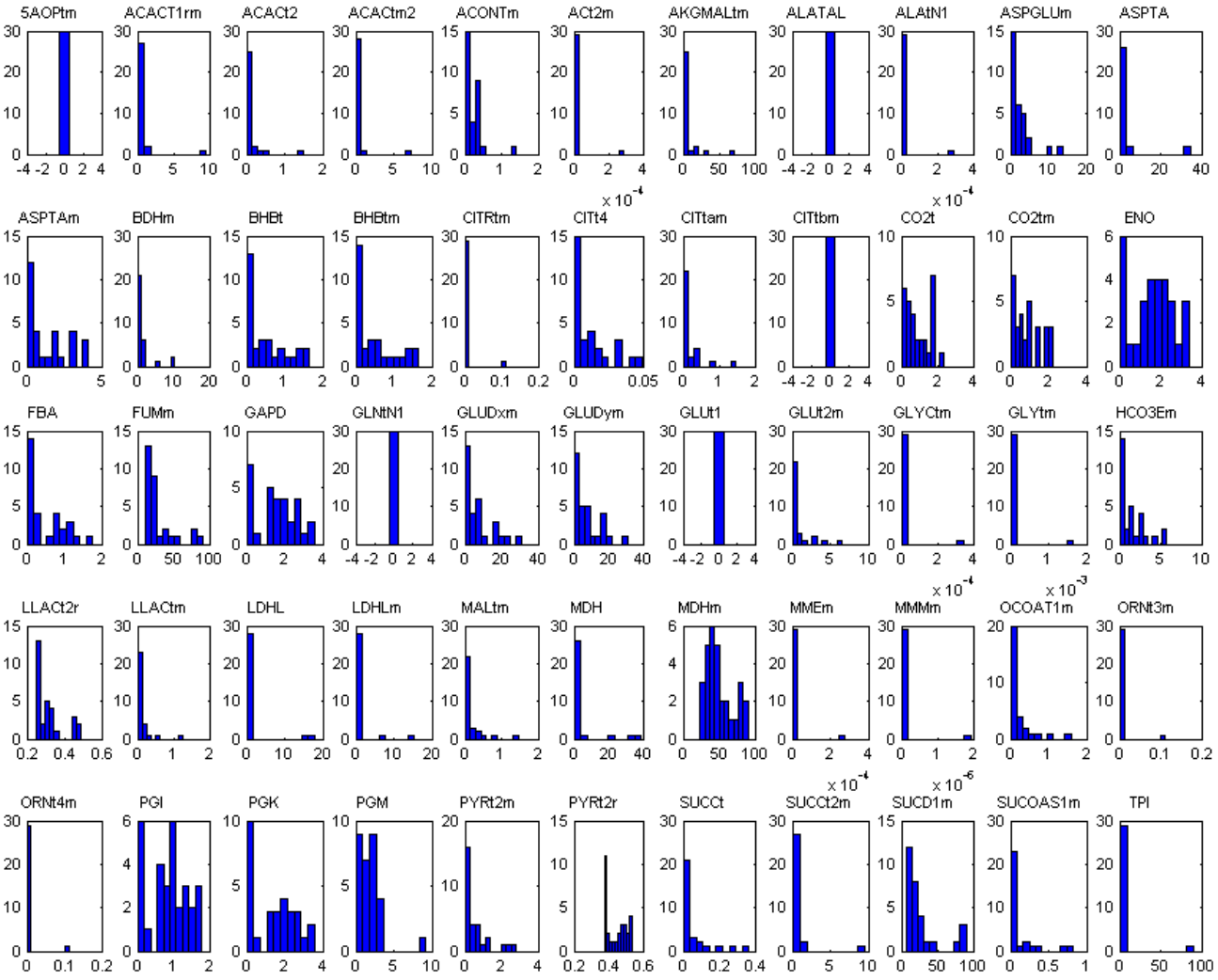

SUPPLEMENTAL DATA S3:
Estimated net fluxes and exchange fluxes of reactions in the network

Index: index of the reactions in the Stoichiometric (S) matrix
Equation: [c], [e], and [m] stand for cytosolic, extracellular, and mitochondrial localization. Metabolites in the left hand side of the arrow have negative coefficients (including exchange reactions), while those in the right side have positive coefficients in the S matrix. See the list of metabolite (below) for definition of metabolite abbreviations
Net: calculated net fluxes
SD: standard deviation of calculated net fluxes computed across all locally optimal solutions with sufficiently small Error values (values of the objective function)
Exch: calculated exchange fluxes. NTR: exchange fluxes not tracked.

INDEX	NAME	EQUATION	PATHWAY	NET	SD	EXCH
1	DMatp	[c]: atp + h2o → atp + h + pi	Demand	16.63	2.30	
2	DMpheme	[m]: pheme →	Demand	0.00	0.00	
3	DMphoslipid	[m]: 0.18 clpn_m + 0.43 pc_m + 0.34 pe_m →	Demand	0.00	0.00	
4	EX12dgr	[e]: 12dgr <==>		0.00	0.00	NTR
5	EXac	[e]: ac <==>		0.00	0.00	NTR
6	EXacac	[e]: acac <==>	Efflux	0.27	0.36	NTR
7	EXalaL	[e]: ala-L <==>		0.00	0.00	NTR
8	EXarachd	[e]: arachd <==>		0.00	0.00	NTR
9	EXbhb	[e]: bhn <==>	Efflux	0.46	0.33	NTR
10	EXbilirub	[e]: bilirub <==>		0.00	0.00	NTR
11	EXchol	[e]: chol <==>		0.00	0.00	NTR
12	EXcit	[e]: cit <==>	Efflux	0.02	0.00	NTR
13	EXco	[e]: co <==>		0.00	0.00	NTR
14	EXco2	[e]: co2 <==>	Efflux	3.22	0.10	NTR
15	EXcoa	[e]: coa <==>		0.00	0.00	NTR
16	EXcrvnc	[e]: crvnc <==>		0.00	0.00	NTR
17	EXfe2	[e]: fe2 <==>		0.00	0.00	NTR
18	EXglc	[e]: glc <==>	Uptake	-1.50	0.03	NTR
19	EXglnL	[e]: gln-L <==>		0.00	0.00	NTR
20	EXgluL	[e]: glu-L <==>		0.00	0.00	NTR
21	EXgly	[e]: gly <==>		0.00	0.00	NTR
22	EXglyc	[e]: glyc <==>		0.00	0.00	NTR
23	EXh	[e]: h <==>	Efflux	3.54	0.05	NTR
24	EXh2o	[e]: h2o <==>	Efflux	3.68	0.25	NTR
25	EXhdca	[e]: hdca <==>		0.00	0.00	NTR
26	EXhdcea	[e]: hdcea <==>		0.00	0.00	NTR
27	EXlacL	[e]: lac-L <==>	Efflux	2.10	0.05	NTR
28	EXna1	[e]: na1 <==>		0.00	0.00	NTR
29	EXnh4	[e]: nh4 <==>		0.00	0.00	NTR
30	EXo2	[e]: o2 <==>	Uptake	-5.49	0.06	NTR
31	EXocdca	[e]: ocdca <==>		0.00	0.00	NTR
32	EXocdcea	[e]: ocdcea <==>	Uptake	-0.30	0.00	NTR
33	EXocdcya	[e]: ocdcya <==>		0.00	0.00	NTR
34	EXocta	[e]: octa <==>		0.00	0.00	NTR
35	EXpi	[e]: pi <==>		0.00	0.00	NTR
36	EXppa	[e]: ppa <==>		0.00	0.00	NTR
37	EXps	[e]: ps <==>		0.00	0.00	NTR
38	EXpyr	[e]: pyr <==>	Efflux	0.62	0.00	NTR
39	EXsucc	[e]: succ <==>	Efflux	0.01	0.00	NTR

59	ALATA_L	[c] : akg + ala-L <==> glu-L + pyr	Amino acid	0.00	0.00	0.00
64	ASNNm	[m] : asn-L + h2o --> asp-L + nh4	Amino acid	0.00	0.00	
154	GLNS	[c] : atp + glu-L + nh4 --> adp + gln-L + h + pi	Amino acid	5.40	5.98	
159	GLUDxm	[m] : glu-L + h2o + nad <==> akg + h + nadh + nh4	Amino acid	0.00	0.00	4.87
160	GLUDym	[m] : glu-L + h2o + nadp <==> akg + h + nadph + nh4	Amino acid	0.00	0.00	5.05
161	GLUNm	[m] : gln-L + h2o --> glu-L + nh4	Amino acid	5.40	5.98	
47	ACITL	[c] : atp + cit + coa --> accoa + adp + oaa + pi	Anaplerosis	0.00	0.00	
194	LDH_L	[c] : lac-L + nad <==> h + nadh + pyr	Anaplerosis	-1.89	0.26	0.11
195	LDH_Lm	[m] : lac-L + nad <==> h + nadh + pyr	Anaplerosis	-0.21	0.25	0.03
200	ME2m	[m] : mal-L + nadp --> co2 + nadph + pyr	Anaplerosis	0.00	0.00	
221	PCm	[m] : atp + hco3 + pyr --> adp + h + oaa + pi	Anaplerosis	0.02	0.00	
224	PEPCKm	[m] : gtp + oaa --> co2 + gdp + pep	Anaplerosis	0.00	0.00	
141	FAOXC80	[m] : (3) coa + (3) fad + (3) h2o + (3) nad + occoa --> (4) accoa + (3) fadh2 + (3) h + (3) nadh	FA oxidation	0.00	0.00	
135	FAOXC160	[m] : (7) coa + (7) fad + (7) h2o + (7) nad + pmtcoa --> (8) accoa + (7) fadh2 + (7) h + (7) nadh	FA oxidation	0.30	0.00	
136	FAOXC180	[m] : coa + fad + h2o + nad + stcoa --> accoa + fadh2 + h + nadh + pmtcoa	FA oxidation	0.00	0.00	
137	FAOXC181	[m] : coa + h2o + nad + odecoa --> accoa + h + nadh + pmtcoa	FA oxidation	0.30	0.00	
138	FAOXC182	[m] : (8) coa + (6) fad + (8) h2o + (8) nad + ocdycacoa --> (9) accoa + (6) fadh2 + (8) h + (8) nadh	FA oxidation	0.00	0.00	
139	FAOXC204	[m] : arachdcoa + (9) coa + (5) fad + (9) h2o + (9) nad --> (10) accoa + (5) fadh2 + (9) h + (9) nadh	FA oxidation	0.00	0.00	
140	FAOXC226	[m] : c226coa + (10) coa + (4) fad + (10) h2o + (10) nad --> (11) accoa + (4) fadh2 + (10) h + (10) nadh	FA oxidation	0.00	0.00	
113	CRNtim	crn[m] --> crn[c]	FA oxidation	0.30	0.00	
134	FACOAL80i	[c] : atp + coa + octa --> amp + occoa + ppi	FA oxidation	0.00	0.00	
211	OCCOAtm	occoa[c] --> occoa[m]	FA oxidation	0.00	0.00	
127	FACOAL160i	[c] : atp + coa + hdca --> amp + pmtcoa + ppi	FA oxidation	0.00	0.00	
76	C160CPT1	[c] : crn + pmtcoa --> coa + pmtcrn	FA oxidation	0.00	0.00	
78	C160CRNt	pmtcrn[c] --> pmtcrn[m]	FA oxidation	0.00	0.00	
77	C160CPT2	[m] : coa + pmtcrn --> crn + pmtcoa	FA oxidation	0.00	0.00	
128	FACOAL161i	[c] : atp + coa + hdcea --> amp + hdcoa + ppi	FA oxidation	0.00	0.00	
79	C161CPT1	[c] : crn + hdcoa --> coa + hdcecrn	FA oxidation	0.00	0.00	
81	C161CRNt	hdcecrn[c] --> hdcecrn[m]	FA oxidation	0.00	0.00	
80	C161CPT2	[m] : coa + hdcecrn --> crn + hdcoa	FA oxidation	0.00	0.00	
129	FACOAL180i	[c] : atp + coa + ocdca --> amp + ppi + stcoa	FA oxidation	0.00	0.00	
82	C180CPT1	[c] : crn + stcoa --> coa + stcrn	FA oxidation	0.00	0.00	
84	C180CRNt	stcrn[c] --> stcrn[m]	FA oxidation	0.00	0.00	
83	C180CPT2	[m] : coa + stcrn --> crn + stcoa	FA oxidation	0.00	0.00	
130	FACOAL181i	[c] : atp + coa + ocdcea --> amp + odecoa + ppi	FA oxidation	0.30	0.00	
85	C181CPT1	[c] : crn + odecoa --> coa + odecrn	FA oxidation	0.30	0.00	
87	C181CRNt	odecrn[c] --> odecrn[m]	FA oxidation	0.30	0.00	
86	C181CPT2	[m] : coa + odecrn --> crn + odecoa	FA oxidation	0.30	0.00	
131	FACOAL182i	[c] : atp + coa + ocdcya --> amp + ocdycacoa + ppi	FA oxidation	0.00	0.00	
88	C182CPT1	[c] : crn + ocdycacoa --> coa + ocdycrn	FA oxidation	0.00	0.00	
90	C182CRNt	ocdycrn[c] --> ocdycrn[m]	FA oxidation	0.00	0.00	
89	C182CPT2	[m] : coa + ocdycrn --> crn + ocdycacoa	FA oxidation	0.00	0.00	
132	FACOAL204i	[c] : arachd + atp + coa --> amp + arachdcoa + ppi	FA oxidation	0.00	0.00	
91	C204CPT1	[c] : arachdcoa + crn --> arachdcrn + coa	FA oxidation	0.00	0.00	
93	C204CRNt	arachdcrn[c] --> arachdcrn[m]	FA oxidation	0.00	0.00	
92	C204CPT2	[m] : arachdcrn + coa --> arachdcoa + crn	FA oxidation	0.00	0.00	
133	FACOAL226i	[c] : atp + coa + crvnc --> amp + c226coa + ppi	FA oxidation	0.00	0.00	
94	C226CPT1	[c] : c226coa + crn --> c226crn + coa	FA oxidation	0.00	0.00	
96	C226CRNt	c226crn[c] --> c226crn[m]	FA oxidation	0.00	0.00	
95	C226CPT2	[m] : c226crn + coa --> c226coa + crn	FA oxidation	0.00	0.00	

182	HEX1	[c] : atp + glc-D --> adp + g6p + h	Glycolysis	1.50	0.03	
226	PGI	[c] : g6p <==> f6p	Glycolysis	1.50	0.03	0.77
225	PFK	[c] : atp + f6p --> adp + fdp + h	Glycolysis	1.50	0.03	
144	FBA	[c] : fdp <==> dhap + g3p	Glycolysis	1.50	0.03	0.35
255	TPI	[c] : dhap <==> g3p	Glycolysis	1.50	0.03	0.77
152	GAPD	[c] : g3p + nad + pi <==> 13dpg + h + nadh	Glycolysis	3.00	0.05	1.37
227	PGK	[c] : 3pg + atp <==> 13dpg + adp	Glycolysis	-3.00	0.05	1.22
228	PGM	[c] : 2pg <==> 3pg	Glycolysis	-3.00	0.05	1.39
125	ENO	[c] : 2pg <==> h2o + pep	Glycolysis	3.00	0.05	1.43
245	PYK	[c] : adp + h + pep --> atp + pyr	Glycolysis	3.00	0.05	
58	ALASm	[m] : gly + h + succoa --> 5aop + co2 + coa	Heme	0.00	0.00	
41	5AOPtm	5aop[c] <==> 5aop[m]	Heme	0.00	0.00	0.00
238	PPBNGS	[c] : (2) 5aop --> h + (2) h2o + ppbng	Heme	0.00	0.00	
183	HMBS	[c] : h2o + (4) ppbng --> hmbil + (4) nh4	Heme	0.00	0.00	
256	UPP3S	[c] : hmbil --> h2o + uppg3	Heme	0.00	0.00	
257	UPPDC1	[c] : (4) h + uppg3 --> (4) co2 + cpppg3	Heme	0.00	0.00	
112	CPPPGO	[c] : cpppg3 + (2) h + o2 --> (2) co2 + (2) h2o + pppg9	Heme	0.00	0.00	
240	PPPG9tm	pppg9[c] <==> pppg9[m]	Heme	0.00	0.00	NTR
241	PPPGOm	[m] : (3) o2 + (2) pppg9 --> (6) h2o + (2) ppp9	Heme	0.00	0.00	
145	FCLTm	[m] : fe2 + ppp9 --> (2) h + pheme	Heme	0.00	0.00	
186	HOXG	[c] : (5) h + (3) nadph + (3) o2 + pheme --> biliverd + co + fe2 + (3) h2o + (3) nadp	Heme	0.00	0.00	
74	BILIRED	[c] : biliverd + h + nadph --> bilirub + nadp	Heme	0.00	0.00	
42	ACACT1rm	[m] : (2) accoa <==> aacoa + coa	Ketone bodies	0.72	0.03	0.24
184	HMGCOASim	[m] : aacoa + accoa + h2o --> coa + h + hmgcoa	Ketone bodies	1.13	0.92	
185	HMGLm	[m] : hmgcoa --> acac + accoa	Ketone bodies	1.13	0.92	
71	BDHm	[m] : bhb + nad <==> acac + h + nadh	Ketone bodies	-0.46	0.33	0.50
215	OCOAT1m	[m] : acac + succoa <==> aacoa + succ	Ketone bodies	0.41	0.91	0.13
45	ACCOACm	[m] : accoa + atp + hco3 --> adp + h + malcoa + pi	Lipid	4.50	4.60	
46	ACCOALm	[m] : atp + coa + ppa --> amp + ppcoa + ppi	Lipid	0.00	0.00	
50	ACSm	[m] : ac + atp + coa --> accoa + amp + ppi	Lipid	0.00	0.00	
99	CHOLK	[c] : atp + chol --> adp + cholp + h	Lipid	0.00	0.00	
115	CSNAT2m	[m] : coa + pcrn <==> crn + ppcoa	Lipid	0.00	0.00	NTR
116	CSNATm	[m] : acrn + coa <==> accoa + crn	Lipid	0.00	0.00	NTR
142	FAS160N	[c] : (8) accoa + (7) atp + (6) h + h2o + (14) nadph --> (7) adp + (8) coa + hdca + (14) nadp + (7) pi	Lipid	0.00	0.00	
143	FASYN_H	[m] : (0.2) arachdcoa + (0.05) c226coa + (0.05) hdcoa + (0.3) ocdycacoa + (0.1) odecoa + (0.2) pmtcoa + (0.1) stcoa --> facoa_hg	Lipid	0.00	0.00	
197	MCD	[m] : h + malcoa --> accoa + co2	Lipid	4.50	4.60	
201	MMEm	[m] : mmcoa-R <==> mmcoa-S	Lipid	0.00	0.00	0.00
202	MMMm	[m] : mmcoa-R <==> succoa	Lipid	0.00	0.00	0.00
239	PPCOACm	[m] : atp + hco3 + ppcoa --> adp + h + mmcoa-S + pi	Lipid	0.00	0.00	
167	GLYKm	[m] : atp + glyc --> adp + glyc3p + h	Lipid	0.00	0.00	
151	G3PDm	[m] : fad + glyc3p --> dhap + fadh2	Lipid	0.00	0.00	
150	G3PATm_HG	[m] : facoa_hg + glyc3p --> 1ag3p + coa	Lipid	0.00	0.00	
55	AGATm_HG	[m] : 1ag3p + facoa_hg --> coa + pa	Lipid	0.00	0.00	
122	DASYN	[m] : ctp + h + pa <==> cdpdag + ppi	Lipid	0.00	0.00	NTR
219	PAPA	[m] : h2o + pa --> 12dgr + pi	Lipid	0.00	0.00	
126	ETHAPT	[m] : 12dgr + cdpea <==> cmp + h + pe	Lipid	0.00	0.00	NTR
242	PSD	[m] : h + ps --> co2 + pe	Lipid	0.00	0.00	
98	CHLPCTD	[c] : cholp + ctp + h --> cdpchol + ppi	Lipid	0.00	0.00	
121	DAGCPT	[c] : 12dgr + cdpchol --> cmp + h + pc	Lipid	0.00	0.00	
220	PCHOLP	[m] : h2o + pc --> chol + h + pa	Lipid	0.00	0.00	
230	PGSA	[m] : cdpdag + glyc3p --> cmp + h + pgp	Lipid	0.00	0.00	
229	PGPP	[m] : h2o + pgp --> pg + pi	Lipid	0.00	0.00	
106	CLPNS	[m] : cdpdag + pg <==> clpn + cmp + h	Lipid	0.00	0.00	NTR

65	ASPGLUm	asp-L[m] + glu-L[c] + h[c] <==> asp-L[c] + glu-L[m] + h[m]	Mal-Asp Shuttle	1.11	0.25	1.30
66	ASPTA	[c] : akg + asp-L <==> glu-L + oaa	Mal-Asp Shuttle	1.11	0.25	1.14
198	MDH	[c] : mal-L + nad <==> h + nadh + oaa	Mal-Asp Shuttle	-1.11	0.25	1.01
57	AKGMALtm	akg[m] + mal-L[c] <==> akg[c] + mal-L[m]	Mal-Asp Shuttle	1.11	0.25	2.02
67	ASPTAm	[m] : akg + asp-L <==> glu-L + oaa	Mal-Asp Shuttle	-1.11	0.25	1.02
53	ADK1	[c] : amp + atp <==> (2) adp	Nucleotide	0.30	0.00	NTR
54	ADK1m	[m] : amp + atp <==> (2) adp	Nucleotide	0.00	0.00	NTR
68	ATPCTPm	[m] : amp + ctp <==> atp + cmp	Nucleotide	0.00	0.00	NTR
105	CK	[m] : atp + creat <==> adp + pcreat	Nucleotide	0.00	0.00	NTR
120	CYTK1	[c] : atp + cmp <==> adp + cdp	Nucleotide	0.00	0.00	NTR
204	NDPK1	[c] : atp + gdp <==> adp + gtp	Nucleotide	-1.08	0.92	NTR
205	NDPK3	[c] : atp + cdp <==> adp + ctp	Nucleotide	0.00	0.00	NTR
175	H2CO3Dm	[m] : co2 + h2o <==> h2co3	Others	0.00	0.00	NTR
176	H2OD	[c] : h2o <==> h + oh1	Others	0.00	0.00	NTR
179	HCO3Em	[m] : co2 + h2o <==> h + hco3	Others	4.52	4.60	1.02
234	PPA	[c] : h2o + ppi --> h + (2) pi	Others	0.30	0.00	
235	PPAm	[m] : h2o + ppi --> h + (2) pi	Others	0.00	0.00	
203	NADH2-u10m	(5) h[m] + nadh[m] + q10[m] --> (4) h[c] + nad[m] + q10h2[m]	OxPhos	7.56	0.18	
252	SUCD3-u10m	[m] : fadh2 + q10 <==> fad + q10h2	OxPhos	3.59	0.05	NTR
119	CYOR-u10m	(2) ficytC[m] + (2) h[m] + q10h2[m] --> (2) focytC[m] + (4) h[c] + q10[m]	OxPhos	11.15	0.13	
118	CYOOm3	(4) focytC[m] + (7.92) h[m] + o2[m] --> (4) ficytC[m] + (4) h[c] + (1.96) h2o[m] + (0.02) o2-[m]	OxPhos	5.58	0.06	
69	ATPS4m	adp[m] + (4) h[c] + pi[m] --> atp[m] + (3) h[m] + h2o[m]	OxPhos	23.08	3.94	
158	GLUCYS	[c] : atp + cys-L + glu-L --> adp + glucys + h + pi	ROS	0.00	0.00	
173	GTHS	[c] : atp + glucys + gly --> adp + gthrd + h + pi	ROS	0.00	0.00	
172	GTHRDt	atp[c] + gthrd[c] + h2o[c] <==> adp[c] + gthrd[m] + h[c] + pi[c]	ROS	0.00	0.00	NTR
171	GTHPm	[m] : (2) gthrd + h2o2 <==> gthox + (2) h2o	ROS	0.01	0.02	NTR
170	GTHOm	[m] : gthox + h + nadph --> (2) gthrd + nadp	ROS	0.01	0.02	
248	SPODMm	[m] : (2) h + (2) o2- --> h2o2 + o2	ROS	0.06	0.00	
97	CATm	[m] : (2) h2o2 --> (2) h2o + o2	ROS	0.03	0.01	
254	THD1m	h[c] + nadh[m] + nadp[m] <==> h[m] + nad[m] + nadph[m]	ROS	0.00	0.01	NTR
223	PDHm	[m] : coa + nad + pyr --> accoa + co2 + nadh	TCA cycle	0.25	0.00	
117	CSm	[m] : accoa + h2o + oaa --> cit + coa + h	TCA cycle	1.51	0.05	
48	ACONTm	[m] : cit <==> icit	TCA cycle	1.49	0.05	0.17
189	ICDHxm	[m] : icit + nad --> akg + co2 + nadh	TCA cycle	1.49	0.05	
190	ICDHym	[m] : icit + nadp --> akg + co2 + nadph	TCA cycle	0.00	0.01	
56	AKGDm	[m] : akg + coa + nad --> co2 + nadh + succoa	TCA cycle	1.49	0.05	
253	SUCOAS1m	[m] : coa + gtp + succ <==> gdp + pi + succoa	TCA cycle	-1.08	0.92	0.04
251	SUCD1m	[m] : fad + succ <==> fadh2 + fum	TCA cycle	1.49	0.05	20.41
148	FUMm	[m] : fum + h2o <==> mal-L	TCA cycle	1.49	0.05	21.62
199	MDHm	[m] : mal-L + nad <==> h + nadh + oaa	TCA cycle	2.60	0.23	46.10
60	ALAt4	ala-L[e] + na1[e] --> ala-L[c] + na1[c]	Transport	0.00	0.00	
61	ALAtN1	ala-L[e] + h[c] + (2) na1[e] <==> ala-L[c] + h[e] + (2) na1[c]	Transport	0.00	0.00	0.00
155	GLNt4	gln-L[e] + na1[e] --> gln-L[c] + na1[c]	Transport	0.00	0.00	
156	GLNtN1	gln-L[e] + h[c] + (2) na1[e] <==> gln-L[c] + h[e] + (2) na1[c]	Transport	0.00	0.00	0.00
162	GLUt1	glu-L[e] + h[c] + (2) na1[e] <==> glu-L[c] + h[e] + (2) na1[c]	Transport	0.00	0.00	0.00
164	GLUt4	glu-L[e] + na1[e] --> glu-L[c] + na1[c]	Transport	0.00	0.00	
168	GLYt4	gly[e] + na1[e] --> gly[c] + na1[c]	Transport	0.00	0.00	
102	CITt4	cit[e] <==> cit[c]	Transport	-0.02	0.00	0.01

153	GLCt1	glc-D[e] --> glc-D[c]	Transport	1.50	0.03	
192	L-LACt2r	h[e] + lac-L[e] <==> h[c] + lac-L[c]	Transport	-2.10	0.05	0.30
247	PYRt2r	h[e] + pyr[e] <==> h[c] + pyr[c]	Transport	-0.62	0.00	0.43
249	SUCCt	succ[e] <==> succ[c]	Transport	-0.01	0.00	0.03
62	ARACHDt	arachd[e] --> arachd[c]	Transport	0.00	0.00	
114	CRVNCt	crvnc[e] --> crvnc[c]	Transport	0.00	0.00	
180	HDCAt	hdca[e] --> hdca[c]	Transport	0.00	0.00	
181	HDCEAt	hdcea[e] --> hdcea[c]	Transport	0.00	0.00	
212	OCDCAt	ocdca[e] --> ocdca[c]	Transport	0.00	0.00	
213	OCDCEAt	ocdcea[e] --> ocdcea[c]	Transport	0.30	0.00	
214	OCDCYAt	ocdcya[e] --> ocdcya[c]	Transport	0.00	0.00	
40	12DGRt2	12dgr[e] --> 12dgr[c]	Transport	0.00	0.00	
43	ACACt2	acac[e] + h[e] <==> acac[c] + h[c]	Transport	-0.27	0.36	0.03
51	ACt2	ac[e] + h[e] --> ac[c] + h[c]	Transport	0.00	0.00	
72	BHBt	bhb[e] + h[e] <==> bhb[c] + h[c]	Transport	-0.46	0.33	0.35
100	CHOLt4	chol[e] + na1[e] <==> chol[c] + na1[c]	Transport	0.00	0.00	NTR
165	GLYCt1	glyc[e] --> glyc[c]	Transport	0.00	0.00	
187	Ht	h[c] <==> h[e]	Transport	0.09	0.00	NTR
216	OCTAt3	octa[e] --> octa[c]	Transport	0.00	0.00	
236	PPAt	ppa[e] --> ppa[c]	Transport	0.00	0.00	
243	PSt2	ps[e] <==> ps[c]	Transport	0.00	0.00	NTR
75	BILIRUBt	bilirub[c] --> bilirub[e]	Transport	0.00	0.00	
107	CO2t	co2[e] <==> co2[c]	Transport	-3.22	0.10	0.84
109	COAt	coa[e] <==> coa[c]	Transport	0.00	0.00	NTR
111	COt	co[c] <==> co[e]	Transport	0.00	0.00	NTR
146	FE2t1	fe2[e] <==> fe2[c]	Transport	0.00	0.00	NTR
177	H2Ot	h2o[e] <==> h2o[c]	Transport	-3.68	0.25	NTR
191	Kt1r	k[e] <==> k[c]	Transport	0.00	0.00	NTR
206	NH4t	nh4[e] <==> nh4[c]	Transport	0.00	0.00	NTR
208	NaKt	atp[c] + h2o[c] + (2) k[e] + (3) na1[c] --> adp[c] + h[c] + (2) k[c] + (3) na1[e] + pi[c]	Transport	0.00	0.00	
209	O2t	o2[e] <==> o2[c]	Transport	5.49	0.06	NTR
233	PIt2r	h[e] + pi[e] <==> h[c] + pi[c]	Transport	0.00	0.00	NTR
63	ARGtm	arg-L[c] + h[m] <==> arg-L[m] + h[c]	Mito transport	0.00	0.00	NTR
101	CITRtm	citr-L[m] <==> citr-L[c]	Mito transport	0.01	0.03	0.00
157	GLNtm	gln-L[c] --> gln-L[m]	Mito transport	5.40	5.98	
163	GLUt2m	glu-L[c] + h[c] <==> glu-L[m] + h[m]	Mito transport	-5.40	5.98	0.35
169	GLYtm	gly[c] <==> gly[m]	Mito transport	0.00	0.00	0.00
217	ORNt3m	h[c] + orn[m] <==> h[m] + orn[c]	Mito transport	-0.01	0.03	0.00
218	ORNt4m	citr-L[c] + h[c] + orn[m] <==> citr-L[m] + h[m] + orn[c]	Mito transport	0.01	0.03	0.00
103	CITtam	cit[c] + mal-L[m] <==> cit[m] + mal-L[c]	Mito transport	-0.02	0.00	0.07
104	CITtbm	cit[c] + pep[m] <==> cit[m] + pep[c]	Mito transport	0.00	0.00	0.00
149	FUMtm	fum[c] + pi[m] <==> fum[m] + pi[c]	Mito transport	0.00	0.00	NTR
193	L-LACtm	h[c] + lac-L[c] <==> h[m] + lac-L[m]	Mito transport	-0.21	0.25	0.03
196	MALtm	mal-L[c] + pi[m] <==> mal-L[m] + pi[c]	Mito transport	-0.02	0.00	0.07
246	PYRt2m	h[c] + pyr[c] <==> h[m] + pyr[m]	Mito transport	0.49	0.25	0.33
250	SUCCt2m	pi[m] + succ[c] <==> pi[c] + succ[m]	Mito transport	-0.01	0.00	0.07
108	CO2tm	co2[c] <==> co2[m]	Mito transport	-3.22	0.10	0.77
147	FE2tm	fe2[c] + h[c] --> fe2[m] + h[m]	Mito transport	0.00	0.00	
178	H2Otm	h2o[c] <==> h2o[m]	Mito transport	-17.61	2.38	NTR
188	Htm	h[c] --> h[m]	Mito transport	8.78	12.95	
207	NH4tm	nh4[c] <==> nh4[m]	Mito transport	-5.40	5.98	NTR
210	O2tm	o2[c] <==> o2[m]	Mito transport	5.49	0.06	NTR
232	PIt2m	h[c] + pi[c] <==> h[m] + pi[m]	Mito transport	19.61	6.04	NTR
44	ACACtm2	acac[c] + h[c] <==> acac[m] + h[m]	Mito transport	-0.27	0.36	0.04
49	ACRNtm	acrn[c] --> acrn[m]	Mito transport	0.00	0.00	
52	ACt2m	ac[c] + h[c] <==> ac[m] + h[m]	Mito transport	0.00	0.00	0.00

73	BHBtm	bhb[c] + h[c] <==> bhb[m] + h[m]	Mito transport	-0.46	0.33	0.32
110	COAtm	coa[c] <==> coa[m]	Mito transport	0.00	0.00	NTR
166	GLYCtm	glyc[c] <==> glyc[m]	Mito transport	0.00	0.00	0.00
222	PCt2m	pc[c] --> pc[m]	Mito transport	0.00	0.00	
237	PPAtm	ppa[c] --> ppa[m]	Mito transport	0.00	0.00	
244	PSt2m	ps[c] --> ps[m]	Mito transport	0.00	0.00	
70	ATPtm	adp[c] + atp[m] --> adp[m] + atp[c]	Mito transport	18.55	5.99	
123	DNC1C	atp[m] + cdp[c] <==> atp[c] + cdp[m]	Mito transport	0.00	0.00	NTR
124	DNC1G	atp[m] + gdp[c] <==> atp[c] + gdp[m]	Mito transport	0.00	0.00	NTR
174	GTPtm	gdp[c] + gtp[m] --> gdp[m] + gtp[c]	Mito transport	1.08	0.92	
231	PHEMEt	pheme[m] <==> pheme[c]	Mito transport	0.00	0.00	NTR

List of metabolites in the network

Index: Index of the metabolite in the S matrix
Abbr.: (c), (e), and (m) stand for cytosolic, extracellular, and mitochondrial localization of the metabolite
Num. of Carbon: The number of carbon atoms, whose labeling patterns are tracked in the model; DE: metabolites are dead ends in the network; eff DE: metabolite is effectively a dead end as it only participate in reactions with other dead ends; NA: isotopomers of the metabolites are not tracked in the model.

Index	Abbr.	Name	Compartment	Num of Carbon
1	12dgr(c)	1,2-Diacylglycerol	Cytosol	NA
2	13dpg(c)	3-Phospho-D-glyceroyl phosphate	Cytosol	3
3	2pg(c)	D-Glycerate 2-phosphate	Cytosol	3
4	3pg(c)	3-Phospho-D-glycerate	Cytosol	3
5	5aop(c)	5-Amino-4-oxopentanoate	Cytosol	5
6	ac(c)	Acetate	Cytosol	2
7	acac(c)	Acetoacetate	Cytosol	4
8	accoa(c)	Acetyl-CoA	Cytosol	eff DE
9	acrn(c)	O-Acetylcarnitine	Cytosol	DE
10	adp(c)	ADP	Cytosol	NA
11	akg(c)	2-Oxoglutarate	Cytosol	5
12	ala-L(c)	L-Alanine	Cytosol	3
13	amp(c)	AMP	Cytosol	NA
14	arachd(c)	arachidonic acid	Cytosol	NA
15	arachdcoa(c)	C20:4-CoA	Cytosol	NA
16	arachdcrn(c)	C20:4 carnitine	Cytosol	NA
17	arg-L(c)	L-Arginine	Cytosol	DE
18	asp-L(c)	L-Aspartate	Cytosol	4
19	atp(c)	ATP	Cytosol	NA
20	bhb(c)	(R)-3-Hydroxybutanoate	Cytosol	4
21	bilirub(c)	Bilirubin	Cytosol	NA
22	biliverd(c)	Biliverdin	Cytosol	NA
23	c226coa(c)	cervonyl coenzyme A	Cytosol	NA
24	c226crn(c)	cervonyl carnitine	Cytosol	NA
25	cdp(c)	CDP	Cytosol	NA
26	cdpchol(c)	CDPcholine	Cytosol	NA
27	chol(c)	Choline	Cytosol	NA
28	cholp(c)	Choline phosphate	Cytosol	NA
29	cit(c)	Citrate	Cytosol	6
30	citr-L(c)	L-Citrulline	Cytosol	6
31	cmp(c)	CMP	Cytosol	NA
32	co(c)	Carbon monoxide	Cytosol	eff DE

33	co2(c)	CO2	Cytosol		1
34	coa(c)	Coenzyme A	Cytosol	NA	
35	cpppg3(c)	Coproporphyrinogen III	Cytosol	NA	
36	crn(c)	L-Carnitine	Cytosol	NA	
37	crvnc(c)	cervonic acid	Cytosol	NA	
38	ctp(c)	CTP	Cytosol	NA	
39	cys-L(c)	L-Cysteine	Cytosol	DE	
40	dhap(c)	Dihydroxyacetone phosphate	Cytosol		3
41	f6p(c)	D-Fructose 6-phosphate	Cytosol		6
42	fdp(c)	D-Fructose 1,6-bisphosphate	Cytosol		6
43	fe2(c)	Fe2+	Cytosol	NA	
44	fum(c)	Fumarate	Cytosol	DE	
45	g3p(c)	Glyceraldehyde 3-phosphate	Cytosol		3
46	g6p(c)	D-Glucose 6-phosphate	Cytosol		6
47	gdp(c)	GDP	Cytosol	NA	
48	glc-D(c)	D-Glucose	Cytosol		6
49	gln-L(c)	L-Glutamine	Cytosol		5
50	glu-L(c)	L-Glutamate	Cytosol		5
51	glucys(c)	gamma-L-Glutamyl-L-cysteine	Cytosol	NA	
52	gly(c)	Glycine	Cytosol		2
53	glyc(c)	Glycerol	Cytosol		3
54	gthrd(c)	Reduced glutathione	Cytosol	NA	
55	gtp(c)	GTP	Cytosol	NA	
56	h(c)	H+	Cytosol	NA	
57	h2o(c)	H2O	Cytosol	NA	
58	hdca(c)	Hexadecanoate (n-C16:0)	Cytosol	NA	
59	hdcea(c)	Hexadecenoate (n-C16:1)	Cytosol	NA	
60	hdcecrn(c)	Hexadecenoyl-CoA (nC16:1)	Cytosol	NA	
61	hdcoa(c)	Hexadecenoyl-CoA (n-C16:1CoA)	Cytosol	NA	
62	hmbil(c)	Hydroxymethylbilane	Cytosol	NA	
63	k(c)	potassium	Cytosol	NA	
64	lac-L(c)	L-Lactate	Cytosol		3
65	mal-L(c)	L-Malate	Cytosol		4
66	na1(c)	Sodium	Cytosol	NA	
67	nad(c)	Nicotinamide adenine dinucleotide	Cytosol	NA	
68	nadh(c)	Nicotinamide adenine dinucleotide - reduced	Cytosol	NA	
69	nadp(c)	Nicotinamide adenine dinucleotide phosphate	Cytosol	DE	
70	nadph(c)	Nicotinamide adenine dinucleotide phosphate - reduced	Cytosol	DE	
71	nh4(c)	Ammonium	Cytosol	NA	
72	o2(c)	O2	Cytosol	NA	
73	oaa(c)	Oxaloacetate	Cytosol		4
74	occoa(c)	Octanoyl-CoA (n-C8:0CoA)	Cytosol	NA	
75	ocdca(c)	octadecanoate (n-C18:0)	Cytosol	NA	
76	ocdcea(c)	octadecenoate (n-C18:1)	Cytosol	NA	
77	ocdcya(c)	octadecadienoate (n-C18:2)	Cytosol	NA	
78	ocdycacoa(c)	Octadecynoyl-CoA (n-C18:2CoA)	Cytosol	NA	
79	ocdycrn(c)	octadecynoyl carnitine	Cytosol	NA	
80	octa(c)	octanoate (n-C8:0)	Cytosol	NA	
81	odecoa(c)	Octadecenoyl-CoA (n-C18:1CoA)	Cytosol	NA	
82	odecrn(c)	octadecenoyl carnitine	Cytosol	NA	
83	oh1(c)	hydroxide ion	Cytosol	DE	
84	orn(c)	Ornithine	Cytosol		5
85	pc(c)	Phosphatidylcholine	Cytosol	NA	
86	pep(c)	Phosphoenolpyruvate	Cytosol		3
87	pheme(c)	Protoheme	Cytosol	NA	
88	pi(c)	Phosphate	Cytosol	NA	
89	pmtcoa(c)	Palmitoyl-CoA (n-C16:0CoA)	Cytosol	NA	

90	pmtcrn(c)	L-Palmitoylcarnitine	Cytosol	NA	
91	ppa(c)	Propionate (n-C3:0)	Cytosol		3
92	ppbng(c)	Porphobilinogen	Cytosol	NA	
93	ppi(c)	Diphosphate	Cytosol	NA	
94	pppg9(c)	Protoporphyrinogen IX	Cytosol	NA	
95	ps(c)	Phosphatidylserine	Cytosol	NA	
96	pyr(c)	Pyruvate	Cytosol		3
97	stcoa(c)	Stearoyl-CoA (n-C18:0CoA)	Cytosol	NA	
98	stcrn(c)	stearoylcarnitine	Cytosol	NA	
99	succ(c)	Succinate	Cytosol		4
100	uppg3(c)	Uroporphyrinogen III	Cytosol	NA	
101	12dgr(e)	1,2-Diacylglycerol	Extracellular	NA	
102	ac(e)	Acetate	Extracellular		2
103	acac(e)	Acetoacetate	Extracellular		4
104	ala-L(e)	L-Alanine	Extracellular		3
105	arachd(e)	arachidonic acid	Extracellular	NA	
106	bhb(e)	(R)-3-Hydroxybutanoate	Extracellular		4
107	bilirub(e)	Bilirubin	Extracellular	NA	
108	chol(e)	Choline	Extracellular	NA	
109	cit(e)	Citrate	Extracellular		6
110	co(e)	Carbon monoxide	Extracellular	eff DE	
111	co2(e)	CO2	Extracellular		1
112	coa(e)	Coenzyme A	Extracellular	NA	
113	crvnc(e)	cervonic acid	Extracellular	NA	
114	fe2(e)	Fe2+	Extracellular	NA	
115	glc-D(e)	D-Glucose	Extracellular		6
116	gln-L(e)	L-Glutamine	Extracellular		5
117	glu-L(e)	L-Glutamate	Extracellular		5
118	gly(e)	Glycine	Extracellular		2
119	glyc(e)	Glycerol	Extracellular		3
120	h(e)	H+	Extracellular	NA	
121	h2o(e)	H2O	Extracellular	NA	
122	hdca(e)	Hexadecanoate (n-C16:0)	Extracellular	NA	
123	hdcea(e)	Hexadecenoate (n-C16:1)	Extracellular	NA	
124	k(e)	potassium	Extracellular	NA	
125	lac-L(e)	L-Lactate	Extracellular		3
126	na1(e)	Sodium	Extracellular	NA	
127	nh4(e)	Ammonium	Extracellular	NA	
128	o2(e)	O2	Extracellular	NA	
129	ocdca(e)	octadecanoate (n-C18:0)	Extracellular	NA	
130	ocdcea(e)	octadecenoate (n-C18:1)	Extracellular	NA	
131	ocdcya(e)	octadecadienoate (n-C18:2)	Extracellular	NA	
132	octa(e)	octanoate (n-C8:0)	Extracellular	NA	
133	pi(e)	Phosphate	Extracellular	NA	
134	ppa(e)	Propionate (n-C3:0)	Extracellular		3
135	ps(e)	Phosphatidylserine	Extracellular	NA	
136	pyr(e)	Pyruvate	Extracellular		3
137	succ(e)	Succinate	Extracellular		4
138	12dgr(m)	1,2-Diacylglycerol	Mitochondria	NA	
139	1ag3p(m)	1-Acyl-sn-glycerol 3-phosphate	Mitochondria	NA	
140	5aop(m)	5-Amino-4-oxopentanoate	Mitochondria		5
141	aacoa(m)	Acetoacetyl-CoA	Mitochondria		4
142	ac(m)	Acetate	Mitochondria		2
143	acac(m)	Acetoacetate	Mitochondria		4
144	accoa(m)	Acetyl-CoA	Mitochondria		2
145	acrn(m)	O-Acetylcarnitine	Mitochondria	eff DE	
146	adp(m)	ADP	Mitochondria	NA	

147	akg(m)	2-Oxoglutarate	Mitochondria		5
148	amp(m)	AMP	Mitochondria	NA	
149	arachdcoa(m)	C20:4-CoA	Mitochondria	NA	
150	arachdcrn(m)	C20:4 carnitine	Mitochondria	NA	
151	arg-L(m)	L-Arginine	Mitochondria	DE	
152	asn-L(m)	L-Asparagine	Mitochondria	DE	
153	asp-L(m)	L-Aspartate	Mitochondria		4
154	atp(m)	ATP	Mitochondria	NA	
155	bhb(m)	(R)-3-Hydroxybutanoate	Mitochondria		4
156	c226coa(m)	cervonyl coenzyme A	Mitochondria	NA	
157	c226crn(m)	cervonyl carnitine	Mitochondria	NA	
158	cdp(m)	CDP	Mitochondria	DE	
159	cdpdag(m)	CDPdiacylglycerol	Mitochondria	NA	
160	cdpea(m)	CDPethanolamine	Mitochondria	DE	
161	chol(m)	Choline	Mitochondria	DE	
162	cit(m)	Citrate	Mitochondria		6
163	citr-L(m)	L-Citrulline	Mitochondria		6
164	clpn(m)	Cardiolipin	Mitochondria	NA	
165	cmp(m)	CMP	Mitochondria	NA	
166	co2(m)	CO2	Mitochondria		1
167	coa(m)	Coenzyme A	Mitochondria	NA	
168	creat(m)	Creatine	Mitochondria	DE	
169	crn(m)	L-Carnitine	Mitochondria	NA	
170	ctp(m)	CTP	Mitochondria	NA	
171	dhap(m)	Dihydroxyacetone phosphate	Mitochondria	DE	
172	facoa_hg(m)	Weighted average acyl group of HepG2 cell phospholipid	Mitochondria	NA	
173	fad(m)	Flavin adenine dinucleotide oxidized	Mitochondria	NA	
174	fadh2(m)	Flavin adenine dinucleotide reduced	Mitochondria	NA	
175	fe2(m)	Fe2+	Mitochondria	NA	
176	ficytC(m)	Ferricytochrome c	Mitochondria	NA	
177	focytC(m)	Ferrocytochrome C	Mitochondria	NA	
178	fum(m)	Fumarate	Mitochondria		4
179	gdp(m)	GDP	Mitochondria	NA	
180	gln-L(m)	L-Glutamine	Mitochondria		5
181	glu-L(m)	L-Glutamate	Mitochondria		5
182	gly(m)	Glycine	Mitochondria		2
183	glyc(m)	Glycerol	Mitochondria		3
184	glyc3p(m)	Glycerol 3-phosphate	Mitochondria		3
185	gthox(m)	Oxidized glutathione	Mitochondria	NA	
186	gthrd(m)	Reduced glutathione	Mitochondria	NA	
187	gtp(m)	GTP	Mitochondria	NA	
188	h(m)	H+	Mitochondria	NA	
189	h2co3(m)	carbonic acid	Mitochondria	DE	
190	h2o(m)	H2O	Mitochondria	NA	
191	h2o2(m)	Hydrogen peroxide	Mitochondria	NA	
192	hco3(m)	Bicarbonate	Mitochondria		1
193	hdcecrn(m)	Hexadecenoyl-CoA (nC16:1)	Mitochondria	NA	
194	hdcoa(m)	Hexadecenoyl-CoA (n-C16:1CoA)	Mitochondria	NA	
195	hmgcoa(m)	Hydroxymethylglutaryl-CoA	Mitochondria		6
196	icit(m)	Isocitrate	Mitochondria		6
197	lac-L(m)	L-Lactate	Mitochondria		3
198	mal-L(m)	L-Malate	Mitochondria		4
199	malcoa(m)	Malonyl-CoA	Mitochondria		3
200	mmcoa-R(m)	(R)-Methylmalonyl-CoA	Mitochondria		4
201	mmcoa-S(m)	(S)-Methylmalonyl-CoA	Mitochondria		4
202	nad(m)	Nicotinamide adenine dinucleotide	Mitochondria	NA	

203	nadh(m)	Nicotinamide adenine dinucleotide - reduced	Mitochondria	NA	
204	nadp(m)	Nicotinamide adenine dinucleotide phosphate	Mitochondria	NA	
205	nadph(m)	Nicotinamide adenine dinucleotide phosphate - reduced	Mitochondria	NA	
206	nh4(m)	Ammonium	Mitochondria	NA	
207	o2(m)	O2	Mitochondria	NA	
208	o2s(m)	Superoxide anion	Mitochondria	NA	
209	oaa(m)	Oxaloacetate	Mitochondria		4
210	occoa(m)	Octanoyl-CoA (n-C8:0CoA)	Mitochondria	NA	
211	ocdycacoa(m)	Octadecynoyl-CoA (n-C18:2CoA)	Mitochondria	NA	
212	ocdycrn(m)	octadecynoyl carnitine	Mitochondria	NA	
213	odecoa(m)	Octadecenoyl-CoA (n-C18:1CoA)	Mitochondria	NA	
214	odecrn(m)	octadecenoyl carnitine	Mitochondria	NA	
215	orn(m)	Ornithine	Mitochondria		5
216	pa(m)	Phosphatidate	Mitochondria	NA	
217	pc(m)	Phosphatidylcholine	Mitochondria	NA	
218	pcreat(m)	Phosphocreatine	Mitochondria	DE	
219	pcrn(m)	propionyl-carnitine	Mitochondria	DE	
220	pe(m)	Phosphatidylethanolamine	Mitochondria	NA	
221	pep(m)	Phosphoenolpyruvate	Mitochondria		3
222	pg(m)	Phosphatidylglycerol	Mitochondria	NA	
223	pgp(m)	Phosphatidylglycerophosphate	Mitochondria	NA	
224	pheme(m)	Protoheme	Mitochondria	NA	
225	pi(m)	Phosphate	Mitochondria	NA	
226	pmtcoa(m)	Palmitoyl-CoA (n-C16:0CoA)	Mitochondria	NA	
227	pmtcrn(m)	L-Palmitoylcarnitine	Mitochondria	NA	
228	ppa(m)	Propionate (n-C3:0)	Mitochondria		3
229	ppcoa(m)	Propanoyl-CoA	Mitochondria		3
230	ppi(m)	Diphosphate	Mitochondria	NA	
231	ppp9(m)	Protoporphyrin	Mitochondria	NA	
232	pppg9(m)	Protoporphyrinogen IX	Mitochondria	NA	
233	ps(m)	Phosphatidylserine	Mitochondria	NA	
234	pyr(m)	Pyruvate	Mitochondria		3
235	q10(m)	Ubiquinone-10	Mitochondria	NA	
236	q10h2(m)	Ubiquinol-10	Mitochondria	NA	
237	stcoa(m)	Stearoyl-CoA (n-C18:0CoA)	Mitochondria	NA	
238	stcrn(m)	stearoylcarnitine	Mitochondria	NA	
239	succ(m)	Succinate	Mitochondria		4
240	succoa(m)	Succinyl-CoA	Mitochondria		4